The Who, What, When of Cosmic Reionization: Constraints on the Timeline and Responsible Sources

By

Patricia Marie Bolan

Dissertation

Submitted in partial satisfaction of the requirements for the degree of

Doctor of Philosophy

in

Physics

in the

Office of Graduate Studies

of the

University of California

Davis

Approved:

Professor Maruša Bradač, Chair

Professor Tucker Jones

Professor Chris Fassnacht

Committee in Charge

2023

Contents

List of Figures

List of Tables

Abstract of the Dissertation

The Who, What, When of Cosmic Reionization: Constraints on the Timeline and Responsible Sources

The *Epoch of Reionization* marks the period following the Dark Ages, the era beginning 400,000 years after the Big Bang in which neutral hydrogen permeated the Universe. Reionization is defined as the period of cosmic history in which this hydrogen went from being neutral to ionized, ending at around redshift $z \sim 6$, or about 1 billion years after the Big Bang. This period marks the last major phase change of hydrogen in the intergalactic medium. It was also a time of significant galaxy and structure formation, when the first sources of light emerged. These nascent galaxies were likely major contributors to reionization, emitting large amounts of high energy photons which escaped into the intergalactic medium and began to ionize the vast sea of neutral hydrogen. However, beyond these facts, there are still many open questions surrounding the Epoch of Reionization. Some of the remaining uncertainties concern how quickly the transition occurred, what the key drivers were in the process, and what their physical properties are.

This dissertation aims to address some of these lingering questions. In this work, I use a large sample of characteristically faint, gravitationally lensed, high-redshift galaxies in order to constrain both the timeline of reionization and the physical properties of the ionizing sources. The galaxies used in this sample have deep photometric data in multiple bands from the *Hubble Space Telescope* and *Spitzer Space Telescope*, as well as followup spectroscopy from the *Keck Observatory*. The high quality of photometric data provides good constraints on the redshift and physical properties of galaxies in our sample, even if they lack spectroscopic confirmation. The sample is comprised of ~ 250 Lyman Break galaxy candidates within the redshift range $5 < z < 8.2$, spanning the heart and tail ends of the reionization era. Galaxy candidates for spectroscopic follow-up were chosen after multiband photometric observations were completed. These were selected via the Lyman Break technique and using constraints on the redshift probability distribution created from each galaxy's photometry. Follow-up spectroscopic observations resulted in 38 spectroscopically confirmed galaxies via detection of the Lyman-α (Lyα, 1216Å) line, and constraints on Lyα strength for the rest

of the sample. For all analyses done in this dissertation, I use these ~ 250 galaxies lying in the redshift range $5 < z < 8.2$ in order to constrain both the timeline of reionization and the stellar and UV properties of galaxies in this epoch.

I begin in Chapter 2 with a study on the timeline of reionization using Lyα emission properties from galaxies during and directly after the process was complete. In this work, I compare the prevalence and strength of Lyα emission from galaxies within the Epoch of Reionization ($z \sim 6.7$ and $z \sim 7.6$) and when reionization was mostly, if not entirely, complete ($z \sim 6$). I compare the UV luminosities and β slopes of the samples at the different redshifts and show that the distributions are similar for both properties. As the galaxies all have similar UV properties, and therefore are likely at similar states of interstellar medium evolution, we attribute any difference in the Lyα equivalent width distributions to the evolving opacity of hydrogen in the intergalactic medium. The results of this study, which are consistent with other works, suggest a rapid and fairly late reionization scenario. This work is published in the *Monthly Notices of the Royal Astronomical Society*, (Bolan et al., 2022).

In Chapter 3, I present an analysis of the physical properties of the galaxy sample as well as the results of a search for CIII] emission in confirmed Lyα emitters, which can provide systemic redshifts as well as a basis on which to infer metallicities and ionization parameters. For each of the galaxies, I calculate UV luminosity and β slope, the slope in the UV spectrum of a galaxy redward of Lyα emission, from photometry as well as estimate stellar mass, star formation rate, specific star formation rate, and mass-weighted age via spectral energy density fitting. For galaxies with Lyα emission, I look at the equivalent width (EW) of the emission line as a function of all of these properties to see if there are any correlations. I also compare the distributions of each of these properties for Lyα emitters against nonemitters to see if there are significant physical differences between these groups of galaxies. I find no statistically significant relationships between Lyα EW and any physical properties, nor any significant difference between the sample of Lyα emitters and nonemitters.

In Chapter 4, I provide a summary. Using a sample of gravitationally lensed, intrinsically faint, high-redshift galaxies, I infer a timeline of cosmic reionziation and characterize the

physical properties of typical galaxies from the era. These analyses are especially important as we enter an era of massive space and ground based observatories, such as the *James Webb Space Telescope*, the *European Extremely Large Telescope*, the *Thirty Meter Telescope*, and the *Giant Magellan Telescope*. The work done in this dissertation improves the of knowledge on high-redshift galaxies to guide future observations and surveys. With deep data on large samples of early galaxies from these observatories, a detailed timeline of reionization can be even further constrained, as well as the properties of the main drivers of the process.

Acknowledgments

The work done in this dissertation would not have been possible without the academic, moral, and emotional support of so many people. The first people I would like to thank are my parents. Without your constant support and encouragement of pursuing physics, I would not be finishing this dissertation today. Thank you for prioritizing my education throughout my life, setting up a remote observing station for me to control a huge telescope in Hawaii from my childhood bedroom when I got stuck home with covid, and for the endless love. And of course to my sister Katie, thank you for all the days home alone as kids watching space documentaries which lit the astrophysics curiosity in me and for all the physics homework help from high school to college. I never take for granted how amazing it is to have an older sister in the same field, especially when we get to talk physics at the dinner table and see the glaze of confusion appear on our parents' faces.

To my adviser, Maruša Bradač, thank you so much for instilling confidence in me, modelling work-life balance, and allowing me to pursue a Ph.D. in a nontraditional manner. I always tell people how lucky I am to have a thesis adviser who gets me. Thank you for showing me that you can be a badass outdoors-woman and successful physicist all at the same time and for trusting me to stay on top of my work while roaming around the US and Canada (and taking off for the occassional pow day). My other "unofficial" adviser, Brian Lemaux, may not be my PI on paper, but was absolutely imperative to my success. Brian, I can't thank you enough for supporting me not only as a student but as a person over the past five years. Thank you for giving me constructive criticism when I needed it, lifting me out of dark emotional places, telling me when I need to push and when I need to take a break, and for jumping off cliffs in Hawaii with me. Thanks as well to all the others in the department who took me under their wing and helped me with paper writing, coding, and galaxy physics, especially Victoria, Tucker, Chris, David, Debora, Priti, and Kelsey.

Thank you to the buddies and pals I made in Davis, from the physics and astronomy department and beyond. Mac, Emae, Conner, and Alyssa, thank you for being the girl gang I never knew I needed until we all came together. To the fellas (and Julie) in my cohort, Pratik, Tyler, Arsalan, Yash, Jake, Sid, Karthik, Patrick, Ethan, and more, thank you

for the late night first year homework sessions, secret santas, and friendsgivings. Thanks as well to the other folks who I kept coming back to town for even after leaving Davis, especially David and Lynn. I also owe so much to the Utah friends, even though we may be all spread out across the west these days, for all the climbing, backpacking, and general outdoor shenanigans throughout the years: Caleb, Justina, Caroline, Mary, Ryan, Emily, Brian, Glynis, Dan, Alyssa and Ty, and Ben. I also would not have gotten through some days without all the amazing dogs I've been lucky to watch and foster throughout my Ph.D., especially Stella, Poe, Hachi, and Firb.

The people I've met on the road and in my second home in South Lake Tahoe since moving into the van two and a half years ago have provided me with crucial perspective on the work I do. Thank you to all the friends I made from Colorado to Nova Scotia to Alaska for not only the endless practice in talking about my research to non-astronomers but for expanding my views beyond the academic bubble. And thank you to my little family at Coldwater Brewery for providing the exact opposite kind of stress and convincing me to stay in town for another season. I am so humbled and grateful to have you all in my life.

Chapter 1

An Introduction to Early Galaxies and the Epoch of Reionization

1.1 Cosmic History and Open Questions

A longstanding question is universal to mankind regardless of time period or location: where did we come from? One channel through which humans have attempted to unveil their origin story is the study of astronomy. Even prior to modern scientific advances which allow for detailed insights on the cosmos, civilizations have studied the planets, stars, galaxies, and space itself using primitive methods throughout history. The study of astronomy, whether in ancient cultures or the modern day, extends through the gamut of the human experience; from philosophical musings to the intrinsic drive to discover a sense of place to the pursuit of discovery through the scientific process, humans have looked to space for answers throughout history.

We are now in an age of immense astronomical discovery and growth, fueled by the advent of large-aperture ground and space-based telescopes. With the ever improving technologies available today, astronomers are able to uncover previously inaccessible truths about the Universe and everything within it. This knowledge provides humanity with a framework in which to understand its place in the grand scheme of time and space.

1.1.1 A Brief History of Time

In the past century, our knowledge of the early universe has made extreme advances. The current understanding is that everything as we know it was created in the Big Bang, when the

Universe nearly instantaneously expanded from an exceptionally small size and high density (Tsujikawa, 2003; Martin, 2018; Cimatti et al., 2019; Achúcarro et al., 2022). Within the first few minutes of the Universe's existence, extremely energetic photons and matter radiated in all directions, until everything consisted of a mix of particles, not yet cool enough for atoms to form. Once the Universe expanded and cooled down, the kinetic energy of primordial protons and electrons was low enough that they could bond to form neutral hydrogen atoms (Peebles, 1968; Davé et al., 2001; Wong, 2008). This phenomenon is called recombination, and led to an era called the Dark Ages, named such because of the lack of discrete light sources and opaque nature of the ubiquitous neutral hydrogen (Mo et al., 2010; Cimatti et al., 2019).

During this time, overdensities in the dark matter content of the Universe began to clump together gravitationally, becoming the dark matter halos which would house the first galaxies. Within these overdense regions, the gravitational attraction of dark matter halos, and subsequently baryons, primarily hydrogen and helium, with some trace amounts of lithium, would become strong enough to form the first stars and galaxies. These first light sources emitted energetic photons at high enough energies to ionize neutral hydrogen, at least 13.6eV. This marks the onset of *The Epoch of Reionization* (EoR). The EoR is the period of cosmic history in which the neutral hydrogen in the space between galaxies, or the intergalactic medium (IGM), was ionized by high-energy photons emitted by the first light sources (e.g. McQuinn, 2016; Robertson, 2021).

1.1.2 Open Questions about the Epoch of Reionization

Reionization marks a pivotal change in the Universe, when the IGM went from fully neutral to ionized, yet there are still many open questions about the epoch. The timeline of reionization has yet to be constrained precisely. When did the process begin? How quickly did it occur (Totani et al., 2006; Mason et al., 2018; Hoag et al., 2019; Whitler et al., 2020)? Was it a very patchy process or more relatively smooth (Treu et al., 2012; Pentericci et al., 2014; Mason et al., 2019b)? Complementary to uncertainties on the timing of reionization are questions on who the major sources were: how much did galaxies contribute compared to quasars (Yeh et al., 2023; Fan et al., 2023; Robertson et al., 2023)? Did faint or bright

galaxies release more ionizing radiation (Robertson et al., 2015; Naidu et al., 2020; Lin et al., 2023; Mascia et al., 2023b)? What are the physical properties of a typical emitter of large amounts of ionizing photons (Oyarzún et al., 2017; Jones et al., 2023a)? These remaining mysteries are at the center of many active studies in the field of astronomy today (e.g. Naidu et al., 2020; Robertson, 2021; Treu et al., 2022; Jones et al., 2023a; Finkelstein et al., 2023).

There are several avenues through which to study the EoR. Anything which emitted photons in the early Universe can be helpful in constraining the details of reionization. These light sources can be classified into four categories: photons in the cosmic microwave background (CMB), active galactic nuclei (AGN, or quasars), gamma-ray bursts (GRBs), and galaxies. Observations of the CMB have been helpful to put a timestamp on reionization via the Thomson optical depth, τ, most recently measured by the Planck Collaboration et al. (2020) to be 0.054 ± 0.007. This measure of IGM opacity is determined by observations of polarization anisotropies, which become dampened or extinguished as CMB photons scatter off of free electrons. These observations can give insights on when reionization would have occurred if it were instantaneous, as the optical depth is integrated over the timeline of reionization. However, as the process likely occurred over hundreds of millions of years and was patchy (Mesinger et al., 2015; Robertson, 2021), this metric cannot be used to determine a detailed history of the EoR. An extended model can be assumed to extrapolate a timeline from this method, but it will be inherently model-dependent. A cosmological model must also be assumed in the determination of τ, making it heavily dependent on the assumed parameters.

Quasars are also very useful in EoR studies as their observations can be used to determine the density of neutral hydrogen in the IGM via the Gunn-Peterson trough. This feature is characterized by the suppression of light emission at wavelengths shorter than that of Lyman-α emission (Lyα, 1216Å) in a quasar's rest-frame spectrum due to absorption by neutral hydrogen. Becker et al. (2001) and Fan et al. (2006a) first found that the Gunn-Peterson trough saturates at $z \geq 6$ by measuring that the IGM hydrogen neutral fraction is $< 10^{-3}$ at $z < 6$ via quasar absorption spectra, indicating that reionization was mostly complete at that time. However, at $z > 6$, exploring reionization with quasars is not useful in determining the fraction of neutral hydrogen present in the IGM, as its presence at any

density greater than 1 part in $\sim 10^3$ will absorb photons at wavelengths blueward of Lyα (Gunn & Peterson, 1965; Becker et al., 2001). In addition, quasars are quite rare at high redshifts and likely exist in overdense regions, meaning that any IGM characteristics derived from their properties may not be representative of what is typical. Regardless, observations of quasar spectra and in particular the covering fraction of "dark" pixels in Lyα and Lyβ forests have been instrumental to exploring the tail end of reionization (e.g. D'Aloisio et al., 2015; Zhu et al., 2021, 2022; Bosman et al., 2021; Jin et al., 2023). In a similar vein, studies of GRBs can be useful in constraining the star formation rate density during reionization, and have been used to analyze the emission of ionizing photons (Kistler et al., 2009; Rossi et al., 2022; Trinca et al., 2023).

The last probe of reionization is the one I use in this dissertation: star-forming galaxies. It is unclear when exactly the first galaxies began to form, but recent observations using the *James Webb Space Telescope* (*JWST*) suggest that the first galaxies may have begun to appear within a few hundred million years after the Big Bang, roughly around $z \sim 20$ (e.g. Carnall et al., 2022; Curtis-Lake et al., 2023; Finkelstein et al., 2023; Scholtz et al., 2023). Large samples of confirmed galaxies at $z \geq 5$ serve as a basis through which to study the EoR. These can be used to constrain both the timeline of reionization and which sources were the key players in ionizing the IGM. Both photometric and spectroscopic observations of EoR galaxies are helpful in these studies, and this dissertation presents how galaxy samples can be used to solve the mysteries of cosmic reionization such as the determination of a detailed timeline and characterization of ionizing sources.

1.1.2.1 Who is Emitting the Ionizing Photons?

One of the most prevalent remaining uncertainties surrounding the EoR is who (i.e., which sources) is responsible for emitting the bulk of the photons that ionized the Universe. While there has historically been some contention over the contribution of AGN, many studies have found that it is subdominant (e.g. Hassan et al., 2018; Kulkarni et al., 2019; Dayal et al., 2020; Yeh et al., 2023; Robertson et al., 2023). While AGN emit large amounts of high-energy photons, they are rare at $z \geq 6$, and their luminosity function at these redshifts is still poorly constrained (see Tee et al., 2023). Both observations and simulations point toward galaxies as being the primary drivers of reionization – however, the types

of galaxies emitting the majority of the photons is still debated. Some works, which use models in conjunction with galactic observations, assert that bright galaxies were the ones who reionized the universe, and that it likely occurred rapidly (e.g. Sharma et al., 2016; Naidu et al., 2020, 2022; Lin et al., 2023). Others find that it is more likely to be the far more ubiquitous, characteristically faint galaxies who are responsible for the majority of reionization (e.g. Finkelstein et al., 2019b; Cain et al., 2021; Rosdahl et al., 2022; Mascia et al., 2023a; Simmonds et al., 2023). Some key uncertainties remain which hinder our ability to directly answer these questions, including characterizing the faint end of the luminosity function and determining the escape fraction of ionizing photons from galaxies at high-z (e.g. McGreer et al., 2015; Naidu et al., 2018; Tang et al., 2019; Robertson, 2021; Chisholm et al., 2022). Observations of large samples of galaxies in the EoR and measurements of their ability to emit ionizing photons into the IGM are necessary to identify the key contributors to the process.

The most straightforward way to determine which galaxies dominated reionization is to measure the ionizing production and escape fraction of Lyman Continuum (LyC) photons. However, due to the increasingly neutral IGM at high redshifts, these metrics are not directly measurable in this epoch. Some studies look at low-z analogs where the IGM does not hinder the ability to detect hydrogen transition lines (Vanzella et al., 2016; Izotov et al., 2018; Chisholm et al., 2020; Izotov et al., 2021; Flury et al., 2022). One workaround at high-z is to search for the Lyα line, emitted from hydrogen atoms as an electron transitions from the $n = 2$ to the $n = 1$ level. The strength of this line at lower redshifts has been found to have a correlation with the amount of LyC photons escaping a galaxy (Pahl et al., 2021; Flury et al., 2022; Begley et al., 2022; Saldana-Lopez et al., 2023). Lyα is typically the brightest, and therefore the most accessible, line in the UV, but it is easily scattered by neutral hydrogen, making its detection especially difficult, but not impossible, in the EoR.

1.2 Finding High Redshift Galaxies

Through a combination of deep photometric and spectroscopic observations, galaxies that are very likely or certain to be at high redshifts are identifiable. Since the successful launch and deployment of *JWST*, the number of galaxies being found at $z \geq 5$ is increasing

rapidly. With a large enough sample at our disposal, we can gain insights on both the global and individual properties of galaxies in the EoR and begin to uncover the true nature of reionization.

1.2.1 Photometry

Discovery of high-redshift galaxies is generally done using multi-wavelength imaging. Typically, imaging is the first step to selecting high-z galaxies as it is less time intensive and more efficient than spectroscopy. With observed-frame optical and infrared data, the Lyman-break method (Steidel et al., 1996) can be used to look for galaxies at EoR redshifts. This method consists of finding a characteristic break at the Lyman limit (generally at rest-frame 912Å, but the break is found at the Lyα line for EoR galaxies due to Gunn-Peterson trough absorption), with a lack of flux at shorter wavelengths due to IGM absorption. A blue UV β slope (~ -2) is often looked for as well, but not necessary. This quantity is parameterized as $f_\lambda \propto \lambda^\beta$, where f_λ is the flux density per wavelength and λ is the wavelength, and defines the slope of the UV continuum redward of Lyα emission. Other studies have utilized narrow-band observations, looking for excess flux near the expected wavelength of Lyα, to select high-z candidates (e.g. Nilsson et al., 2007; Laursen et al., 2019; Cabello et al., 2022). With photometry alone, multiband observations can be used to determine a photometric redshift. Depending on the apparent magnitude of the galaxy in question and the quality of observations, photometry can constrain redshifts quite accurately.

With fluxes measured in multiple bands across a range of observed frame wavelengths, we can not only predict the redshifts of galaxies, but measure their stellar properties via spectral energy density (SED) fitting. The sample used in this dissertation has imaging from the *Hubble Space Telescope* (*HST*) and the *Spitzer Space Telescope* (*Spitzer*), which span the rest-frame UV and optical wavelengths of reionization era galaxies. With rest-frame observations at 0.115 - 4.5 μm which include the Lyman break, Lyα line, Balmer and 4000Å break, and Hβ and [OIII] emission lines in many EoR galaxies, SED fitting can accurately estimate stellar masses and star formation rates (SFRs). More sophisticated SED fitting routines allow for non-parametric star formation histories (SFHs) and can use both photometric fluxes and a galaxy's spectrum (e.g. Carnall et al., 2018; Johnson, 2021),

providing more robust results. In addition to estimating physical parameters, photometric constraints can be used to calculate probability distributions of redshifts, or $P(z)$'s. $P(z)$ distributions for the galaxies in this dissertation were determined using Easy and Accurate Redshifts from Yale (EAzY; Brammer et al., 2008) and are used to choose candidates for follow-up spectroscopy to both confirm redshifts and further explore their properties in depth.

1.2.2 Spectroscopy

While photometry alone can give the stellar and UV properties of galaxies, follow-up spectroscopy is useful for multiple reasons, and is essential in some cases. Depending on the depth and wavelength coverage of the imaging, as well as the apparent magnitude of the target, it is possible to tightly constrain the likely redshift and exclude catastrophic failures. But in many cases with high-z galaxies, there is appreciable uncertainty in the $P(z)$ distribution. In some cases, the flux distribution of more nearby dusty galaxies can mimic that of highly redshifted ones, leading to low-z interlopers pervading high-z samples. Spectroscopic confirmation is necessary to determine a galaxy's precise redshift. In the EoR, this is typically done via detection of an emission line. The brightest and therefore generally most accessible line in the rest-frame UV is Lyα. The detection of Lyα at $z > 6$ is complicated by the opacity of the IGM, as it is easily absorbed and scattered by neutral hydrogen. While this is a hindrance for redshift confirmation, it means that when the Lyα is detected, it can be used to study ionizing bubble sizes and kinematics (Sobral et al., 2015; Matthee et al., 2017; Sobral et al., 2018; Mason et al., 2018), and to constrain the neutral hydrogen fraction of the IGM, which is done in this dissertation. In the rest-frame optical, the often brighter Hβ and [OIII] emission lines are detectable for EoR galaxies using $JWST$ and are being used now to spectroscopically confirm galaxy redshifts.

Due to the scattering of Lyα photons by neutral hydrogen, this emission line is often further redshifted with respect to the systemic redshift of the galaxy. A second emission line is often sought in order to measure the systemic redshift of the galaxy, as well as constrain properties including metallicity, ionizing efficiencies, and dust content. In this dissertation, I present a search for the CIII] 1907,1909Å doublet in confirmed Lyα emitters

(LAEs), which has been observed in other high-z galaxies and used to explore their physical makeup in detail (e.g. Stark et al., 2015; Hutchison et al., 2019; Topping et al., 2021; Tang et al., 2023). Radio observations can be used to target the [CII]158μm and [OIII]88μm fine structure lines in reionization era galaxies. Since the successful deployment of $JWST$, detections of rest-frame UV and optical lines at $z \geq 6$ have been rapidly increasing (e.g. Haro et al., 2023; Jung et al., 2023; Trump et al., 2023; Tang et al., 2023; Carnall et al., 2022; Jones et al., 2023b). Such detections have revealed EoR galaxies that contain highly ionized and metal-poor gases, which we expect from the similar faint galaxies used in this dissertation if they indeed were the key drivers of reionization. Large samples of EoR galaxies are currently being assembled from $JWST$ photometric and spectroscopic observations and are expanding upon the repertoire presented in this work and will allow for even tighter constraints on open reionization questions. Even with current and upcoming data from $JWST$, large galaxy samples assembled from ground-based observatories are still relevant in identification of high-z targets and detection of low equivalent width emission lines.

1.2.3 Gravitational Lensing

In addition to the difficulties presented by IGM neutrality, high-redshift galaxies are evasive due to their extreme distances and faint intrinsic luminosities. Studies on the evolution of luminosity function have found an increase in the faint-end slope as redshift increases, indicating that there are orders of magnitude more faint galaxies than bright ones (e.g. Wold et al., 2022). In a blank field survey, the properties of typical high-z galaxies are difficult to attain without extremely time intensive spectroscopy. Luckily, the cosmos provides built-in telescopes throughout space in the form of gravitational lenses.

Gravitational lensing is a cosmological tool in which the fabric of space-time is warped near a massive object. This warping leads to distorted and magnified images of objects which lie behind the lens, which is especially advantageous for the discovery of faint, high-redshift galaxies. The magnification factors of distant galaxies which lie in the fields of massive lensing clusters can reach into the hundreds, increasing the apparent brightness of these sources to levels detectable in reasonable timeframes, typically up to ten hours of integrated observing time on ground-based 10m class telescopes, and often far less. Some of the deepest

observations of lensing cluster fields are the Hubble Frontier Fields (HFF; Lotz et al., 2017), containing six clusters with excellent data in rest-frame optical and infrared wavelengths, five of which are used in this dissertation. Lensing has also been used in many other surveys to aid in the discovery of high-z galaxies (e.g. Postman et al., 2012; Bouwens et al., 2014; Castellano et al., 2016; Huang et al., 2016b; Shipley, 2018; Bradač et al., 2019; Coe et al., 2019; Willott et al., 2022; Treu et al., 2022; Adams et al., 2022; Trussler et al., 2023). Galaxy clusters can reach appreciable masses, up to $\sim 10^{14-15} M_{\odot}$, making them some of nature's most powerful magnifying glasses through which to study faint, high-redshift galaxies.

One complication that comes with studying lensed galaxies is the determination of a magnification factor. This is done by creating a model of the mass in the lensing cluster field, constrained via the locations and redshifts of strongly lensed, multiply imaged systems (e.g., Zwicky, 1937; Strait et al., 2018; Barnacka, 2018). The determination of magnification factors for all galaxy candidates used in this dissertation was done by creating lens models using both strongly and weakly lensed objects in the photometric data, updated as new data was available, ensuring that they are as accurate as possible.

1.3 This dissertation

When combined, photometric and spectroscopic data can be used to gain knowledge on both intrinsically faint, gravitationally lensed galaxies' physical properties and how they impacted the universe in which they formed. In this dissertation, I present multiple ways in which a sample of EoR galaxies can be used to explore both the process itself and the main drivers of it. This work uses a large sample of gravitationally lensed, characteristically faint LBGs in order to begin to answer some of the major questions surrounding reionization. I use these galaxies' photometric and spectroscopic properties, particularly Lyα emission, to infer the neutral hydrogen fraction at various EoR redshifts and explore the physical properties of typical galaxies which are likely to have been at least partially responsible for reionization. In Chapter 2, I present a study published in 2022 which utilizes this sample to constrain the the timeline of reionization (Bolan et al., 2022). This is done by taking two subsamples at EoR redshifts ($z \sim 6.7$ and $z \sim 7.6$) and comparing the Lyα emission properties to a reference sample from the ionized universe ($z \sim 6$), comparing to realistic reionization

simulations, and attributing the differences in Lyα emission to IGM opacity, which can then be used to infer the neutral fraction of hydrogen.

Chapter 3 contains an exploration of the ultraviolet (UV) and stellar properties of the sample. I compare these properties in Lyα emitters versus nonemitters as well as look at the relationships between Lyα strength and physical properties for the emitters. I also discuss the results of a spectroscopic search for CIII] emission in $z \sim 7$ galaxies, which has been submitted to *Monthyl Notices of the Royal Astronomical Society*. In Chapter 4, I summarize and discuss the future of the field, specifially how new observatories will expand upon the work done in this dissertation. Below I give an overview of the observations of these galaxies and how they were discovered.

1.3.1 A Faint Lensed Galaxy Sample from the Epoch of Reionization

The sample used throughout this dissertation is the culmination of decades of work from various scientists, surveys, and collaborations. Each of the LBG candidates has both deep photometry in multiple HST/ACS and HST/WFC3 bands, in addition to *Spitzer* IRAC channels 1 and 2. Spectroscopic follow-up on each candidate was obtained from Keck Observatory. Keck is a pair of twin 10 meter telescopes on the summit of Mauna Kea which has been used to observe a vast range of astronomical objects, from planets within our solar system to some of the most distant galaxies. All of the galaxy candidates are detected in the fields of massive lensing clusters, magnifying their flux by $\sim$ 1-200 times the intrinsic values. This sample is extremely powerful for EoR studies, with a wide range of applications. The largest of its kind, the galaxies span the heart and tail end of reionization ($5 < z < 8.2$) and are characteristically faint ($L \sim 0.1L^*$ where L^* is the characteristic luminosity), extending down to absolute magnitudes of $M_{\rm UV} \sim -14$. As these luminosities are typical at this time, we are able to get a view of what are likely average galaxies. By exploring this sample from multiple angles, I am able to constrain the history of cosmic reionization as well as the likely sources of the majority of ionizing photons.

The original sample selection was from *HST* using a combination of the following filter bands on the Advanced Camera for Surveys (ACS; Sirianni et al., 2005) and Wide Field

Camera (WFC3; Kimble et al., 2008): F435W, F475W, F555W, F606W, F625W, F775W, F850LP, F814W, F105W, F110W, F125W, F140W, and F160W. Out of the ten clusters used, five are Hubble Frontier Fields (HFF, Lotz et al., 2017): A2744, MACS0416, MACS0717, MACS1149, and A370. The sixth HFF cluster is not observable from the northern hemisphere where our spectroscopy was conducted, so is not included. Four clusters come from the Cluster Lensing and Supernova Survey with Hubble (CLASH, Postman et al., 2012), MACS0744, MACS1423, MACS2129, and RXJ1347, and the last, MACS2214, has *HST* imaging from the Spitzer UltRa Faint SUrvey Program (SURFSUP, Bradač et al., 2014). In addition to *HST* imaging from these programs, each cluster has *Spitzer* observations from SURFSUP and the *Spitzer* HFF programs from the 3.6μm and 4.5μm channels on the Infrared Array Camera (IRAC).

After photometry is obtained, the $P(z)$ distributions are determined from flux values in multiple filters, which are used to select candidates for spectroscopic follow-up. We require at least 1% of the $P(z)$ distribution to be within the range where Lyα emission can be detected in order to include it in the sample used for sepctroscopic follow-up. The spectroscopy on this sample was done between 2013-2017 at Keck Observatory. The two main spectrographs used for this dissertation's data are the Keck DEep Imaging Multi-Object Spectrograph (DEIMOS; Faber et al., 2003) and Multi-Object Spectrometer For Infra-Red Exploration (MOSFIRE; McLean et al., 2010). They were configured so that Lyα would be detectable for $5 < z < 7$ galaxies on DEIMOS and $7 < z < 8.2$ galaxies using MOSFIRE. The number of candidates which meet the requisite criteria and have both photometric and spectroscopic observations is 247, comprising the final sample for all the work done in this dissertation.

Chapter 2

Inferring the IGM Neutral Fraction at z $\sim$ 6-8 with Low-Luminosity Lyman Break Galaxies

This chapter is an adapted version of the article titled *Inferring the IGM Neutral Fraction at $z \sim$ 6-8 with Low-Luminosity Lyman Break Galaxies* which was published in Volume 517 of the Monthly Notices of the Royal Astronomical Society (Bolan et al., 2022).

We present a Bayesian inference on the neutral hydrogen fraction of the intergalactic medium (IGM), $\overline{x}_{\rm HI}$, at $z \sim$ 6-8 using the properties of Lyman break galaxies during the Epoch of Reionization. We use large samples of LBG candidates at $5.5 \leq z \leq 8.2$ with spectroscopy from Keck/DEIMOS and Keck/MOSFIRE. For each galaxy, we incorporate either the Lyman-α equivalent width (EW) for detections or the EW limit spectrum for nondetections to parameterize the EW distribution at various ultraviolet brightnesses for a given redshift. Using our reference sample of galaxy candidates from the ionized universe at $z \sim 6.0$, we are able to infer $\overline{x}_{\rm HI}$ at two redshifts: $z \sim 6.7$ and $z \sim 7.6$. This work includes intrinsically faint, gravitationally lensed galaxies at $z \sim 6.0$ in order to constrain the intrinsic faint-end Lyα EW distribution and provide a comparable population of galaxies to counterparts in our sample that are at higher redshift. The inclusion of faint galaxy candidates, in addition to a more sophisticated modelling framework, allows us to better isolate effects of the interstellar medium and circumgalactic medium on the observed Lyman-

α distribution from those of the IGM. We infer an upper limit of $\overline{x}_{\rm HI} \leq 0.25$ (0.44) at $z = 6.7 \pm 0.2$ and a neutral fraction of $\overline{x}_{\rm HI} = 0.83^{+0.08}_{-0.11}$ ($0.83^{+0.11}_{-0.21}$) at $z = 7.6 \pm 0.6$, both within 68% (95%) uncertainty, results which favor a moderately late and fairly rapid reionization.

2.1 Introduction

When the Universe was less than one billion years old, neutral hydrogen atoms in the intergalactic medium (IGM) were ionized by the first light sources. This period of time is called Epoch of Reionization (EoR) and is thought to lie in the redshifts $z \sim 6 - 10$ (Fan et al., 2006a; Schroeder et al., 2013; Hinshaw et al., 2013; McGreer et al., 2015; Planck Collaboration et al., 2020). Some of the biggest open questions in astronomy concern a detailed timeline of the EoR and the sources which are responsible for it, neither of which have been entirely addressed (Robertson et al., 2015; Robertson, 2021). The first light sources in the Universe were young, star-forming galaxies and quasars. The steep faint end of the UV luminosity function (LF) of galaxies suggests that faint galaxies exist in large quantities beyond the observational detection threshold of most surveys of galaxies in this epoch (Bouwens et al., 2015, 2017; Finkelstein et al., 2015; Livermore et al., 2017). Intrinsically faint galaxies are likely promising candidates as the drivers of reionization due to their large numbers if they are capable of producing even modest amounts of escaping ionizing photons (e.g., Marchi et al., 2018; Steidel et al., 2018; Izotov et al., 2018; Finkelstein et al., 2019b; Pahl et al., 2021); however, there is also the possibility of significant ionization from bright galaxies (Mesinger et al., 2015; Naidu et al., 2020; Jung et al., 2020; Endsley et al., 2021).

One powerful probe of the EoR is Lyman-alpha emission (Lyα, 1216 Å), as it is intrinsically the strongest line in the UV. Lyα photons are attenuated by neutral hydrogen, making the line a probe of the ionization state of the IGM as well as properties of the sources which emitted them (Haiman & Spaans, 1999; **?**; McQuinn et al., 2007; Treu et al., 2012; Dijkstra, 2014). Searching for Lyα emission from samples of galaxies with for multiple lines of sight provides a probe of the state of the IGM throughout reionization, provided that the intrinsic emission of Lyα is known. Thus, Lyα emission allows us to trace the volume-averaged neutral hydrogen fraction, $\overline{x}_{\rm HI}$, of the IGM, which starts at $\overline{x}_{\rm HI} = 1$ at the onset of reionization,

and ends at $\simeq 0$ by $z \sim 6$ (Fan et al., 2006b; Miralda-Escude, 1998; Zhu et al., 2021).

The emission properties of Lyα in various populations, both detections and constraints on non-detections, have been used to explore the neutrality of the IGM. A common method used to determine $\overline{x}_{\rm HI}$ at a given redshift is to calculate the Lyα emitter fraction. This quantity is obtained by photometrically selecting a sample of high-redshift candidates via the Lyman break technique and determining the fraction that emit Lyα photons above an equivalent width (EW) threshold via spectroscopic follow up (Vanzella et al., 2011; Caruana et al., 2012; Treu et al., 2013; Caruana et al., 2014; Jung et al., 2020; Fuller et al., 2020; Kusakabe et al., 2020; Wold et al., 2022). Another method is to estimate the Lyα luminosity function at various redshifts and track its evolution (Konno et al., 2014; Morales et al., 2021; Goto et al., 2021; Harish et al., 2021). Both of these methods have yielded results which reflect an increase in Lyα optical depth and from $z = 6$ to $z = 7$ (e.g Kashikawa et al., 2006, 2011; Fontana et al., 2010; Treu et al., 2012; Fuller et al., 2020) as well as a corresponding increase in IGM neutrality (Pentericci et al., 2011, 2014; Ono et al., 2012; Schenker et al., 2012, 2014; Tilvi et al., 2014; Caruana et al., 2014; Hoag et al., 2019; Jung et al., 2020).

These studies have been instrumental in constraining the reionization timeline, but it is difficult to determine a $\overline{x}_{\rm HI}$ value, or even general trend of $\overline{x}_{\rm HI}$, from a simple Lyα emitter fraction, as such a calculation generally ignores many subtleties of how Lya is generated and propagated. Before photons can travel through the IGM, they must escape the interstellar medium (ISM) and circumgalactic medium (CGM) of a galaxy, which affects Lyα photons, as they get scattered by neutral hydrogen in the ISM and CGM before exiting the galaxy. In addition, the large-scale structure of the IGM may have effects on the neutral fraction inference, due to the likely patchiness of neutral hydrogen clouds (Trac et al., 2008; Becker et al., 2018; D'Aloisio et al., 2019).

In the method employed in this paper, introduced by Mason et al. (2018) and Mason et al. (2019a), effects of the ISM and CGM are isolated from those of the IGM by attributing any changes in Lyα emission in the reionizing universe to partial IGM opacity. Results on IGM opacity using this algorithm have been published by Mason et al. (2018, 2019a) and Hoag et al. (2019). In addition, we use simulations with realistic distributions of neutral hydrogen, with galaxies populated with Lyα line profiles from empirical observations, to

investigate the effects of patchiness, providing a path to measuring $\overline{x}_{\rm HI}$.

In this method, we use the full Lyα EW distribution from samples of Lyman Break Galaxies (LBGs) to infer the IGM neutral fraction. By incorporating information from the entire sample, both galaxies with detected Lyα emission and those without, the distribution of the Lyα optical depth and the neutral fraction can be constrained to high precision. We use a Bayesian method to infer $\overline{x}_{\rm HI}$ using a sample of galaxies at various redshifts during the EoR. In this work, we incorporate a new reference sample at $z \sim 6.0$ from Fuller et al. (2020), when reionization is thought to be largely complete, in order to model Lyα EW after its escape from the ISM, but before encountering the IGM. We require galaxies to have similar inherent properties.

An expansive sample of lensed $z \sim 5-7$ galaxies was recently compiled by Fuller et al. (2020), containing spectroscopic data of 198 LBG candidates, 36 of them with Lyα detected in emission. This is the largest faint ($L \sim 0.1L^*$ where L^* is the characteristic luminosity defined by Bouwens et al., 2015) sample at this redshift, assembled from hundreds of orbits on the *Hubble Space Telescope* (*HST*), *Spitzer Space Telescope* (*Spitzer*), and an over four-year long campaign on Keck/DEIMOS (Faber et al., 2003). With over 100 hours of spectroscopy on these LBG candidates, the depth of these data provides excellent constraints on the EW distribution at $5 \leq z \leq 7$. From Fuller et al. (2020), we draw two samples: the reference sample at $z \sim 6.0$ and a set of galaxy candidates at $z \sim 6.7$. This dataset compliments our comparable sample of galaxies firmly in the EoR at $z \sim 7.6$ compiled by Hoag et al. (2019). The three samples used in this work all have similar luminosity distributions comprised of faint luminosities, representing typical galaxies at these redshifts (Hoag et al., 2019). The reference sample is exemplary for characterizing the EW distribution at $z \sim 6.0$ for use in our inference, as the absolute magnitudes of these candidates match those of the higher redshift LBG candidates. This method combines reionization IGM simulations from Mesinger et al. (2016) with empirical models of the effects of the ISM and CGM, determined via the $z \sim 6.0$ reference sample, to infer the global neutral hydrogen fraction from LBG properties. We perform the Bayesian inference of $\overline{x}_{\rm HI}$ at $z \sim 6.7$ and $z \sim 7.6$ using this faint galaxy sample in our ionized baseline in order to compare similar galaxy populations at both redshifts.

The paper is organized as follows. In Section 2, we discuss the data and methods used in

this analysis. Section 3 describes the data analysis involved in comparing the three galaxy samples and the neutral hydrogen fraction inference. In Section 4, we present and discuss our results, and conclusions can be found in Section 5. The following cosmology is used in data analysis throughout the paper: $\Omega_m = 0.3, \Omega_\Lambda = 0.7, H_0 = 70$, and values from Planck Collaboration et al. (2016) for all analysis used to infer the neutral fraction. All magnitudes are given in the AB system, and all equivalent widths are presented in the rest frame.

2.2 Data and Methods

The data used in this analysis come from two sets of observations: a sample of galaxy candidates between $z \sim 5.5 - 6.5$ and $z \sim 6.5 - 7$ (Fuller et al., 2020), and another set between $z \sim 7 - 8.2$ (Hoag et al., 2019). The candidates are detected behind 10 massive lensing clusters, providing a wide range of sightlines which help to alleviate cosmic variance. All imaging data comes from *HST* and *Spitzer* and is summarized in Table 2.1. Five of the clusters are from Hubble Frontier Fields (HFF, Lotz et al., 2017): A2744, MACS0416, MACS0717, MACS1149, and A370. Four clusters come from the Cluster Lensing and Supernova Survey with Hubble (CLASH, Postman et al., 2012), MACS0744, MACS1423, MACS2129, and RXJ1347, and the last, MACS2214, has *HST* imaging from the Spitzer UltRa Faint SUrvey Program (SURFSUP, Bradač et al., 2014). In addition to *HST* imaging from these programs, each cluster has *Spitzer* observations from SURFSUP and the *Spitzer* HFF programs.

The photometric measurements for the Fuller et al. (2020) $z \sim 5.5 - 7$ sample are from the ASTRODEEP (Castellano et al., 2016; Bradač et al., 2019) team for all HFF clusters. For the remaining five clusters, we use an identical method to that of ASTRODEEP for photometric calculations. LBG candidates were selected via the Lyman break technique, and 198 were followed up spectroscopically with Keck/DEIMOS. Most of the 36 LAEs out of this sample have Lyα detections with S/N ¿ 5, with a few below this threshold (S/N generally ≥ 3), but essentially all with $S/N \gtrsim 3$ and a confident visual detection. Details about the sample, photometry, and spectroscopy of the $z \sim 5.5 - 7$ candidates can be found in Fuller et al. (2020).

The galaxies at $z \sim 7 - 8.2$ are taken from Hoag et al. (2019). Nine of the cluster fields, A2744, A370, MACS0416, MACS0744, MACS1149, MACS1423, MACS2129, MACS2214,

Summary of Observations

Cluster Name	Short Name	α_{J2000} (deg)	δ_{J2000} (deg)	$z_{\rm cluster}$	*HST* Imaging (*Spitzer* Imaging)
Abell 2744	A2744	3.5975000	-30.39056	0.308	HFF
Abell 370	A370	39.968000	-1.576666	0.375	HFF
MACSJ0416.1-2403	MACS0416	64.039167	-24.06778	0.420	HFF/CLASH
MACSJ0717.5+0745	MACS0717	109.38167	37.755000	0.548	HFF/CLASH (SURFSUP)
MACSJ0744.8+3927	MACS0744	116.215833	39.459167	0.686	CLASH (SURFSUP)
MACSJ1149.5+2223	MACS1149	177.392917	22.395000	0.544	HFF/CLASH (SURFSUP)
MACSJ1423.8+2404	MACS1423	215.951250	24.079722	0.545	CLASH (SURFSUP)
MACSJ2129.4-0741	MACS2129	322.359208	-7.690611	0.568	CLASH (SURFSUP)
MACSJ2214.9-1359	MACS2214	333.739208	-14.00300	0.500	SURFSUP
RXJ1347.5-1145	RXJ1347	206.87750	-11.75278	0.451	CLASH (SURFSUP)

Table 2.1: Summary of observations for 10 lensing clusters used in this work.

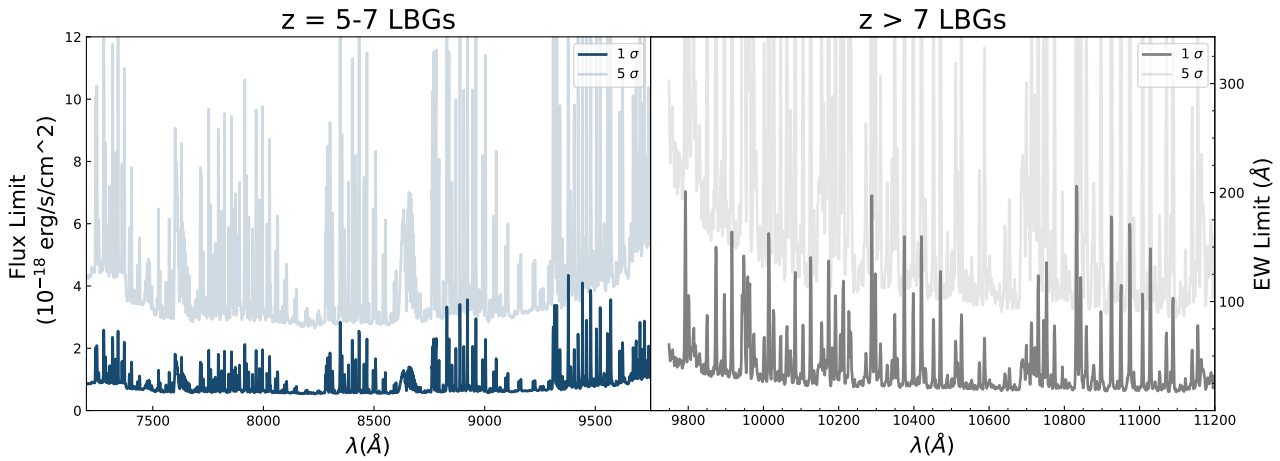

Figure 2.1: Median 1 σ (bold) and 5 σ (faint) upper limits on rest-frame Lyα EW and flux as a function of wavelength for DEIMOS (left) and MOSFIRE (right) non-detections at $z = 5 - 7$ and $z > 7$.

and RXJ1347, are used to search for Lyα emission in the redshift range $z \sim 7 - 8.25$. The photometric data are used to obtain photometric redshift probability distributions, $P(z)$s. For the full $z \sim 7.6$ sample, the photometry and selection criteria (at least 1% probability of being in the redshift range) are identical to those used for the Fuller et al. (2020) sample. More information on the observations of these clusters is detailed in Hoag et al. (2019). In this sample of 68 LBG candidates with spectroscopic data from the KECK Multi-Object Spectrometer for InfraRed Exploration (MOSFIRE; McLean et al., 2010), there are two confident Lyα detections ($S/N \geq 5$ with confident visual detections and characteristic negative traces flanking the central emission feature) and upper limits on line flux and EW for the other galaxies.

For our analysis, we break up the former galaxy sample into two different redshift bins: $z \sim 6.0$ and $z \sim 6.7$ Both samples are drawn from the same set of observations (Fuller et al., 2020). To select galaxies that will serve as the $z \sim 6.0$ reference sample, we make a cut based on the fraction of the $P(z)$ within the redshift range of $P(5.5 < z < 6.5)$ for the $z \sim 6.0$ sample and $P(6.5 < z < 6.9)$ for the $z \sim 6.7$ sample. Requiring that at least 20% of the integrated $P(z)$ lies in these redshift ranges yields a sample of 74 reference galaxies at $z \sim 6.0$ and 28 at $z \sim 6.7$. We note that although the LBG candidates need only have at least 20% of their integrated $P(z)$ in the desired range to be included in our sample, the

inference effectively weights each galaxy's contribution by its fraction of $P(z)$ in the range (see Section 2.3.2). We use $z \sim 6.7$ as the fiducial redshift for candidates with $P(z > 6.5)$ since this is the median of our Lyα detection window for this sample. For the MOSFIRE sample at $z \sim 7.6$, we use the range $P(7 < z < 8.2)$. We test whether selecting samples based on $P(z)$ yields different results on our main analysis from selection based on $z_{\rm phot}$, where $z_{\rm phot}$ is the peak value given by the $P(z)$ distribution. We find that there is very little effect as detailed in Section 2.4.

2.2.1 Flux Calibration

With the three samples of LBG candidates, all with photometric and spectroscopic observations, our goal is to use EW values for LAEs and EW limits for candidates with non-detections to perform the neutral fraction inference. The EW values and limits for the $z \sim 7.6$ sample are computed by Hoag et al. (2019) using the methods described therein. For the $z \sim 5.5 - 7$ galaxies, the EW values of the 36 Lyα detections are calculated by Fuller et al. (2020). Here we determine limits on EW for the non-detections using a method comparable to that used by Fuller et al. (2020) for the detections.

Equivalent width is a relative value which does not require knowledge of a magnification value, nor flux calibration if there is simultaneous detection of continuum. However, in the case of faint galaxies at high redshift, we typically do not detect continuum. Instead, we must first put the error spectrum on an absolute scale, then use it in conjuction with photometry to calculate an EW limit. In the Fuller et al. (2020) sample, there are no sources with detected continuum (see also **?**), so spectrophotometric calibration is necessary for EW calculations for all candidates in the samples. This calibration is therefore determined as follows.

We calculate flux limits for non-LAEs in the DEIMOS samples by calibrating with a bright source with continuum on the same mask to establish an absolute scale, then determine expected slit losses for both the bright object and LBG candidate, based on simulations described in Lemaux et al. (2009). Then we apply these corrections to the noise spectrum, and the flux limit for a given observation, $f_{\rm lim}$, is determined following a method effectively identical to that of Hoag et al. (2019). We find the 1σ Lyα rest-frame EW spectra via:

$$\mathrm{EW}_{lim} = \frac{f_{\mathrm{lim}}(\lambda)}{f_{\mathrm{cont}}(1+z)} \tag{2.1}$$

We determine the continuum flux density, f_{cont}, defined as

$$f_{\mathrm{cont}} = 10^{-0.4(m_{\mathrm{AB}}+48.6)} c/\lambda^2 \tag{2.2}$$

from photometry. In this definition, m_{AB} is the apparent magnitude in the band used to determine continuum flux, typically the F105W band for the $z \sim 5.5$-7 sources, corresponding to an average rest-frame wavelength of $\lambda \sim 1500$ Å. If there is no F105W data available, F125W (rest-frame $\lambda \sim 1800$ Å) is used, and, in a few cases, where there is neither an F150W nor F125W magnitude, F140W (rest-frame $\lambda \sim 2000$ Å) is used. For non-detections, the entire EW spectrum over the DEIMOS window is used in the inference to account for wavelength-dependent sensitivities. We considered using the method of estimating EW by extrapolating the continuum flux to the Lyα wavelength and determining longer wavelength continuum values via the galaxy's β slope, but for this analysis, our uncertainties on magnitudes, and therefore β, are too high to attempt this type of precision correction. Having a large pool of non-detections and their upper limits at various UV magnitudes is helpful to constrain the EW distribution which is used in our neutral fraction inference, as detailed in Mason et al. (2018) and Hoag et al. (2019). In Figure **??**, we show the 1σ and 5σ flux and EW limits for all LBG candidates without spectroscopic detection from both DEIMOS and MOSFIRE.

2.3 Analysis

2.3.1 Comparison of Samples

For the most accurate results in our neutral fraction inference, a good model for intrinsic Lyα emission after escape from the ISM is necessary. Since we compare the Lyα EW distribution at $z \sim 6.0$ to that at higher redshifts, it is important to create a model for intrinsic Lyα emission based on a reference sample that is similar to those at high-z, particularly with comparable luminosities. Hoag et al. (2019) performed this $\overline{x}_{\mathrm{HI}}$ inference based on a sample of galaxies at $z \sim 7.6$ with a bright sample of $z \sim 6.0$ LBG candidates from De Barros et al. (2017) serving as the reference. These 127 galaxies are not lensed and have a median

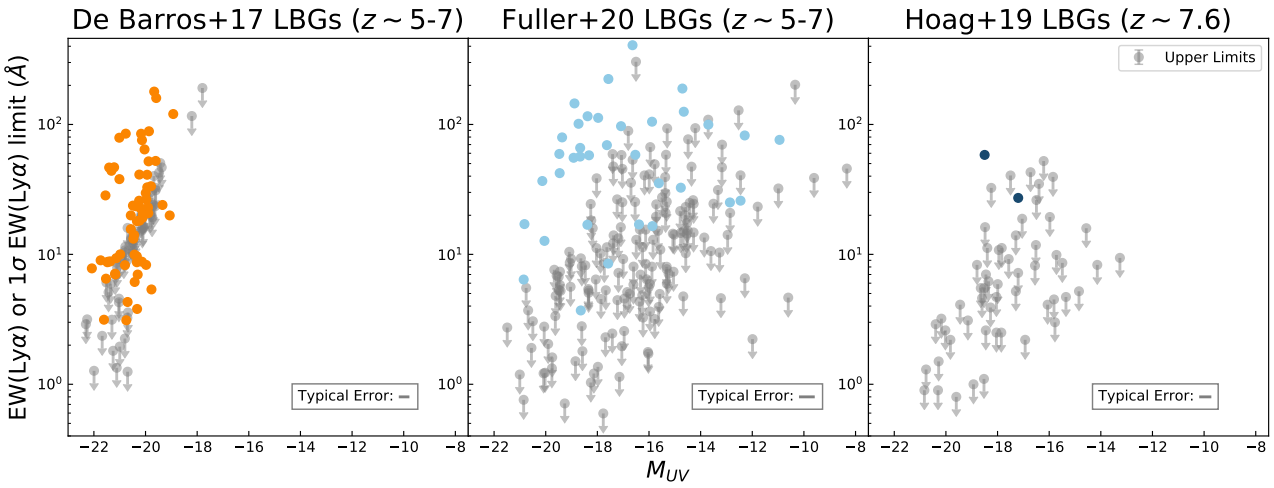

Figure 2.2: Lyα EW value (LAEs, colored dots) or 1σ upper limits (nondetections, grey arrows) of the full samples of LBG candidates from De Barros et al. (2017) (left), Fuller et al. (2020) (center), and Hoag et al. (2019) (right). Typical errors on $M_{\rm UV}$ are shown for each sample.

The $z \sim 5-7$ LBG candidates from Fuller et al. (2020) comprise the largest sample of galaxies at this redshift over these faint UV luminosities. We achieve comparable EW limits to those of De Barros et al. (2017) but for a much fainter sample, making our three samples ($z \sim 6.0$ and $z \sim 6.7$ from Fuller et al., 2020 and $z \sim 7.6$ from Hoag et al., 2019) comparable in $M_{\rm UV}$.

luminosity of $0.6L^*$. We expand upon the previous analysis by including lensed galaxies from Fuller et al. (2020) which represent a more typical, faint population, and have a median luminosity of $0.07L^*$, approximately an order of magnitude fainter than the De Barros et al. (2017) sample. This sample provides a similar population of galaxies to the $z \sim 6.7$ and $z \sim 7.6$ samples, that have median luminosities of $0.08L^*$ and $0.1L^*$, respectively. We show EW values and upper limits as a function of absolute magnitude for all three datasets in Figure 2.2, highlighting the depth and faintness of our new sample. The incorporation of a fainter reference sample of $z \sim 6.0$ LBG candidates as well as a more thorough treatment of the error in our results increase our confidence in the final values.

Using the same reference sample, we infer two neutral fraction values during the EoR: one at $z \sim 6.7$, and another at $z \sim 7.6$. The total sample used to model Lyα EW distribution at $z \sim 6.0$ is comprised of 83 galaxy candidates and 98 confirmed LAEs from Fuller et al. (2020) and De Barros et al. (2017). We do not use the entire Fuller et al. (2020) sample of

198 LBG candidates in this analysis, as we use a stricter $P(z)$ cut, $\int_{z_{\rm low}}^{z_{\rm high}} P(z)dz$ ¿ 20% for the range $5.5 < z < 6.5$.

In this work, we attribute any differences between the observed Lyα EW distribution of the reference sample and the intrinsic distribution at higher redshifts to IGM attenuation. The difference between $z = 6.0$ and $z = 7.6$ is roughly 250 Myr in cosmic time, and the time between $z = 6.0$ and $z = 6.7$ is less than 200 Myr. Studies indicate that the ISM does not evolve much on these timescales (e.g., Wong, 2009); however, we consider how the ISM and consequently the Lyα EW distribution would evolve as a function of redshift. The observed intrinsic Lyα EW distribution is influenced by the ISM; as conditions within a galaxy change, the number of Lyα photons that are able to escape the ISM is affected (**?**Dijkstra, 2014). In the case of ISM evolution over such short time periods, there is some evidence of a positive correlation between Lyα EW and redshift, either from direct Lyα EW vs. redshift measurements or by anticorrelation of Lyα EW with properties such as β slope and $M_{\rm UV}$ which trend toward bluer and fainter values, respectively, with increasing redshift (Hayes et al., 2011; Oyarzún et al., 2017; De Barros et al., 2017). However, recent studies of related Lyα properties indicate that there may not be a significant trend toward higher Lyα EW at increasing redshift from $2 < z < 6$ (Santos et al., 2020), and only a weakly increasing trend of the fraction of Lyα emitters over $3 < z < 6$, with a possible turnover at $z \approx 5.5$ (Kusakabe et al., 2020). Additionally, Caruana et al. (2018) find no trend in Lyα emitter fraction with redshift regardless of Lyα EW threshold, as well as a median Lyα EW that is invariant with redshift, which implies little evolution in Lyα EW distribution over $3 < z < 6$ (though see also Hayes et al. 2021 and references therein). If there is indeed a lack of Lyα EW evolution with redshift, our assumption that the galaxies in the same evolutionary state will have roughly the same Lyα EW distribution at $z \sim 6.0$ as at $z \sim 6.7$ and $z \sim 7.6$ is supported. In any case, the amount of time between our three samples is small enough that any Lyα EW evolution that occurs over these timescales is not significant for our purposes, as it typically takes on the order of 100s of Myrs for the ISM to evolve significantly (Hunter et al., 2022).

To check if our reference sample has similar properties to those at higher redshifts, we compare galaxy properties which give insight into ISM conditions: the UV β slope of the

spectrum redward of Lyα flux and the absolute magnitude, $M_{\rm UV}$. There is evidence that intrinsic Lyα strength (i.e. after escaping the ISM) is correlated with these galaxy properties (**?**Oyarzún et al., 2016, 2017; Reddy et al., 2018). We perform statistical tests on our galaxy populations using these two properties to see if there is significant evidence of the two samples coming from the same parent distribution, as explained next. The more similar the characteristics of the two galaxy populations at different redshifts, the more confident we can be in the results of our inference, as the ISM properties are likely to not differ much.

2.3.1.1 UV Beta Slopes

The UV continuum slope of a galaxy's spectrum, or its β slope, characterizes its flux redward of Lyα emission with the relation $f_\lambda \propto \lambda^\beta$. As mentioned above, β can give insight into a galaxy's physical properties such as star formation rate, metallicity, dust content, and age (e.g., Buat et al., 2012; Yamanaka & Yamada, 2019; Calabrò et al., 2021). To compare the galaxies in our three different redshift ranges, the β slopes are computed for each LBG candidate which has the requisite data. To determine a β slope, at least two magnitude measurements in filters redward of the expected Lyα emission are required. All β slopes are calculated using linear regression fitting of the magnitude values and associated errors from Scikit-Learn (Pedregosa et al., 2018).

For the sample of $z \sim 7.6$ galaxies, the available bands from the *HST* Wide Field Camera 3 (WFC3/IR, Kimble et al., 2008) for calculating β are F125W, F140W, and F160W, as Lyα would fall, when present, within the F105W band. Of the 68 candidates in this sample, 58 have magnitude values in all three bands. Two galaxies have data for only F125W and F160W filters, and we determine the slope using those two points. For the remaining eight galaxies, we do not have sufficient data to measure a β slope. For the 198 LBG candidates at $z \sim 6$, all four of these *HST* WFC3 filters can be, in principle, used in determination of a β slope. For candidates at z ¿ 6.4, Lyα emission would fall within the F105W filter. To check the possible effect this might have on our β slope calculations, we recalculate the β slope omitting the F105W magnitude for the LAEs between $z = 6.4$ and $z = 7.0$ and find that the median beta slope becomes redder by less than 5% on average. This difference is negligible with respect to other uncertainties in the β slope determination such as photometric errors. Since these galaxies are, by definition, not emitting Lyα at a

detectable level in our observations, and there appears to be no appreciate difference in the β slop on average, we choose to retain the F105W filter when calculating β slopes. For the 36 LAEs in the sample, 8 did not have sufficient photometric data to measure a β slope, and of the remaining 28, 26 of them had magnitudes in all four filters, while 2 had magnitudes in just two *HST* filters. Out of 162 galaxies without a Lyα detection, 154 had enough data to determine β, 2 based off of two filters, 17 based off of three filters, and the remaining 135 calculated from all 4 filters. We note that β slope calculations can be influenced by the detection band (F160W for our samples) due to bias from photometric scatter. However, as all our samples use the same band for detection, our β values would all have the same bias, so differentially there is no cause for concern.

Rather than use a sharp cutoff on integrated $P(z)$ when performing statistical tests on galaxy properties between the reference and high-z samples, we adopt a Monte Carlo (MC) method to check the similarity of two samples of candidates. For determining the similarity of β slope distributions, we draw numbers from a random uniform sample between 0 and 1 and check if this number is less than the percentage of $P(z)$ integrated over the desired redshift range ($5.5 < z < 6.5$ for the $z \sim 6.0$ sample, $6.5 < z < 6.9$ for the $z \sim 6.7$ sample, and $7 < z < 8.2$ for the $z \sim 7.6$ sample) for a given MC iteration. If it is, we keep that galaxy's beta slope in the sample. We then perform a two-sample Kolmogorov-Smirnov (KS) test between the β slopes of the remaining $z \sim 6.0$ and $z \sim 6.7$ or ~ 7.6 galaxies, and iterate this process 100 times. The error distribution on β is also sampled over by taking the error from the linear regression fit determining β, multiplying it by a sampled value from a normalized Gaussian distribution, and adding that value to the original β. On every run of this analysis, there are no iterations out of 100 for which we reject the null hypothesis that the two samples are drawn from the same parent distribution at the 3σ level for the $z \sim 6.0$ and $z \sim 6.7$ samples, and ~ 3 rejections for the $z \sim 6.0$ and $z \sim 7.6$ samples. This rejection is based on the output p-value from the KS test, defined as the probability of obtaining test results at least as extreme as the results actually observed under the null hypothesis of identical parent populations. The threshold for rejection is a p-value of less than 0.005. This is true for both the original β values and those modulated by the errors. We conclude that there is no significant evidence to reject the hypothesis that either pair of LBG candidate

samples used in our inference are drawn from the same parent distribution.

For visualization purposes, we plot the distribution of β slopes for galaxies with at least 20% of their $P(z)$ between the desired redshift range for each sample in Figure 2.3. We also include the β slopes from the De Barros et al. (2017) sample which was used as the $z \sim 6.0$ baseline for the inference in Hoag et al. (2019). The entire sample from De Barros et al. (2017) is included as we do not have $P(z)$ information for this data. The p-values displayed on the left of the figure are from KS tests between the $z \sim 6.0$ reference sample and each of the high-z samples, as well as one between the $z \sim 7.6$ sample and the De Barros et al. (2017) $z \sim 6.0$ sample. In all three cases, there is not significant evidence to reject the null hypothesis at the 3σ level. We note that the median β values are consistent with Bouwens et al. (2014) results, as they find that fainter galaxies at a fixed redshift typically have bluer, or more negative, β slopes. While they also find slight reddening with cosmic time at fixed $M_{\rm UV}$, it is not significant, especially the change between $z \sim 7.6$ and $z \sim 6.0$.

2.3.1.2 $M_{\rm uv}$

We perform a similar check on the distribution of absolute magnitude values for the galaxy candidate samples. For each galaxy, $M_{\rm UV}$ is calculated via

$$M_{\rm UV} \approx M_{\rm FUV} = m_{F160W} + 2.5\log_{10}(\mu) - 5(\log_{10}(d_L) - 1) + 2.5\log_{10}(1+z) + 0.12 \quad (2.3)$$

where m_{F160W} is the magnitude in the F160W band, μ is the median magnification value, d_L is luminosity distance in parsecs, and z is the peak redshift of the $P(z)$ distribution, and 0.12 is a K-correction to account for the change in magnitude going from the GALEX NUV to FUV band (see Fuller et al., 2020 for details). The calculation of absolute magnitude for a galaxy depends on its redshift, both directly and through μ and the K-correction. However, the effects of changes to μ and the K-correction based on redshift uncertainties within the desired redshift range for each sample is much smaller than the rest of the uncertainties on $M_{\rm UV}$, hence we assume these to be negligible.

To account for uncertainties in photometric redshift of the non-emitter sample, we sample over the $P(z)$ distribution. An MC approach is utilized again, sampling over the $P(z)$ of each galaxy; if the randomly sampled redshift from the $P(z)$ distribution fits within the desired

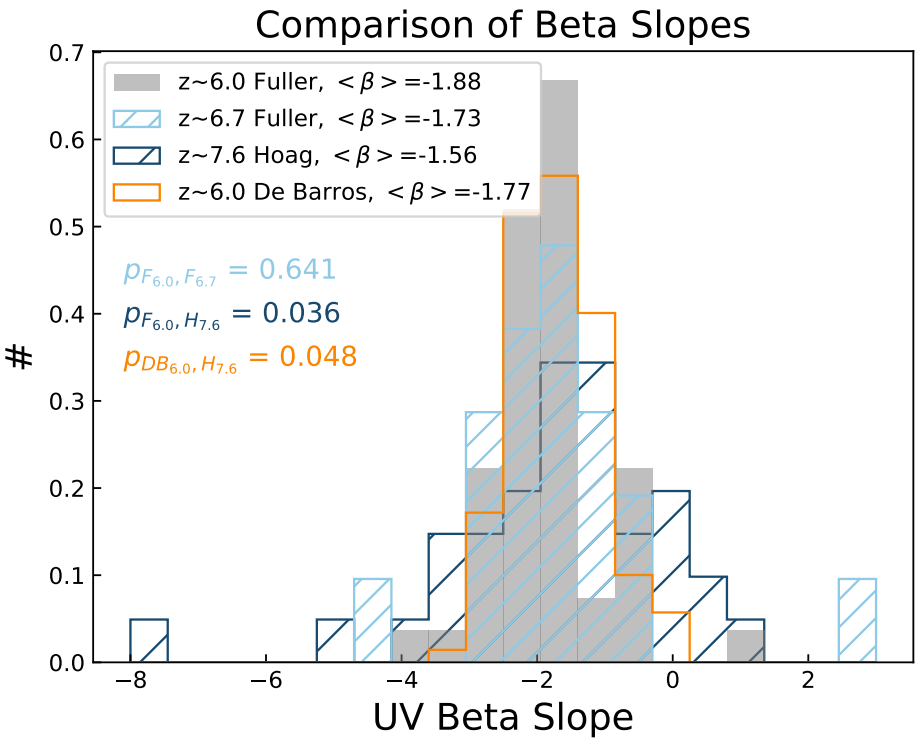

Figure 2.3: A comparison of UV β slope values of the three samples used in this work as well as the $z \sim 6.0$ sample used in the 2019 analysis. This plot and the corresponding p-values only include candidates with $P(z)$ ¿ 20% in the desired redshift range. The p-values from a KS test between the $z \sim 7.6$ and each of the $z \sim 6.0$, as well as that from between the Fuller et al. (2020) 6.0 and $z \sim 6.7$ samples can be seen beneath the legend. For all three pairs of samples, there is not significant evidence to reject the null hypothesis that the distribution comes from the same parent distribution.

range, we keep it for that iteration, compute the $M_{\rm UV}$ based on that value, and perform a KS test between the $M_{\rm UV}$ distributions of the remaining galaxies from the reference $z \sim 6.0$ sample and either $z \sim 6.7$ or $z \sim 7.6$ galaxies. Once again, we also do a test with modulated errors in the same vein as with the β slopes: we multiply the $M_{\rm UV}$ error, with a minimum value of 0.3 magnitudes, by a randomly sampled number from a Gaussian distribution, add that number to the original $M_{\rm UV}$ value, and perform another KS test between the two modulated error samples. This process is then iterated 100 times. For each 100 iterations of the test, there are typically about 5-10 3σ rejections of the null hypothesis for the test between the $z \sim 6.0$ and 7.6 samples, and none for the $z \sim 6.0$ and 6.7 galaxy candidates. Based on the analysis, there is little significant evidence to suggest the populations are from different distributions.

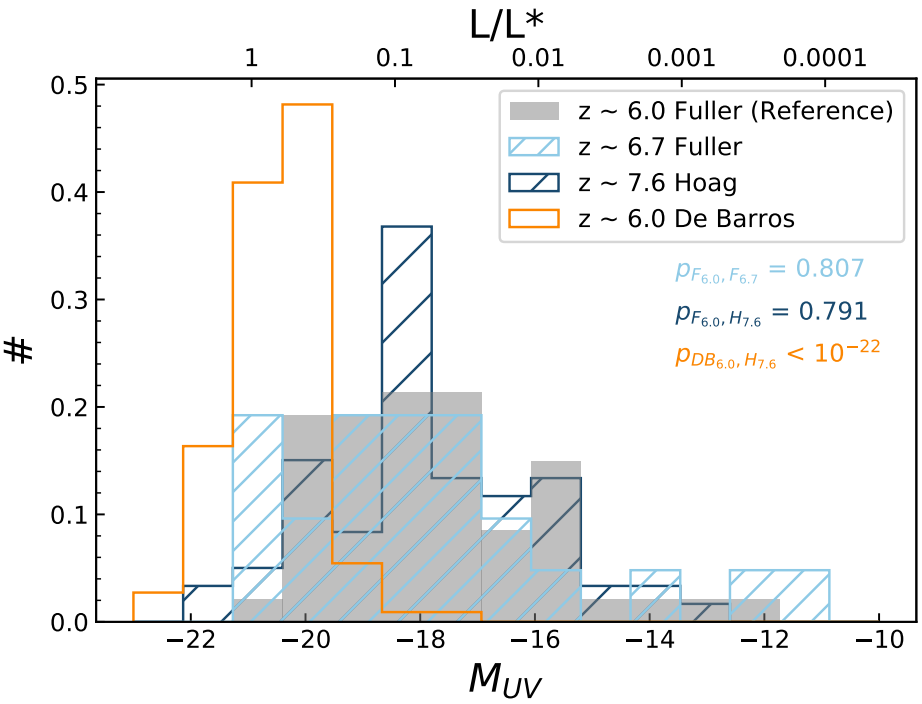

Figure 2.4: A comparison of $M_{\rm UV}$ values of the three samples used in this work: shaded gray ($z \sim 6.0$), hatched light blue (~ 6.7), and dark blue ($z \sim 7.6$) as well as the $z \sim 6.0$ sample used in the 2019 analysis (orange). As with the β slopes, this plot and the corresponding p-values only include candidates with greater than 20% of the $P(z)$ within the desired redshift range. The upper x-axis shows L/L^*, where L^* is the characteristic luminosity of galaxies at z = 6-8. The p-values from a KS test between the $z \sim 6.0$ and $z \sim 6.7$ samples, in addition to that between the $z \sim 7.6$ and each of the $z \sim 6.0$ samples can be seen beneath the legend. There is significant evidence that the De Barros et al. (2017) and Hoag et al. (2019) are not from the same parent distribution. However, there is no indication that the latter and the Fuller et al. (2020) sample are not from the same distribution.

Our reference faint sample is a clear improvement from the bright De Barros et al. (2017) sample for comparison to the $z \sim 7.6$ sample, specifically in terms of absolute magnitudes. The KS test shows that the De Barros et al. (2017) sample and the $z \sim 6.7$ and $z \sim 7.6$ samples are not from the same parent distributions at high confidence. This is shown in Figure 3.3, displaying the distribution of $M_{\rm UV}$ values for all four samples, once again with a $P(z)$ cutoff of $> 20\%$ in the redshift range. It is clear that the Fuller et al. (2020) sample provides a much more comparable population to that of Hoag et al. (2019), as is also evidenced by the KS test results.

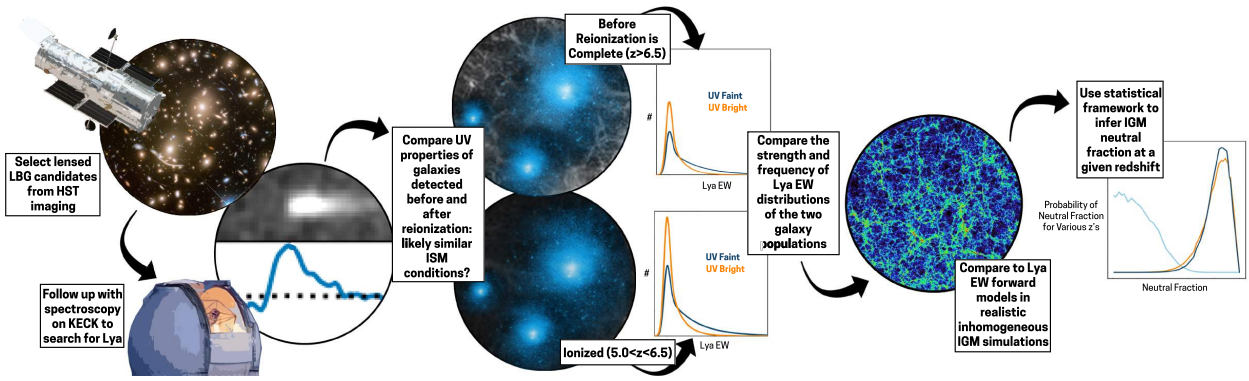

Figure 2.5: An overview of the scientific process used in this analysis. We start by observing the fields of massive galaxy clusters which lens high-z background galaxies. After selecting LBG candidates from these fields, we target them spectroscopically with DEIMOS and MOSFIRE. We then compare the ISM conditions of the LBG populations at different redshifts (section 3.1). Using the differences in Lyα EW distribution during and after reionization, coupled with inhomogeneous IGM simulations (Mesinger et al., 2016) (image from 21cmFAST Mesinger et al., 2011), we use a Bayesian framework (Mason et al., 2018, 2019a) to infer the neutral fraction of hydrogen at various EoR redshifts.

2.3.2 Neutral Fraction Inference

In order to infer the neutral hydrogen fraction, we use the framework described by Mason et al. (2018, 2019a) and refer the reader to these papers for a full description of the methods. A comprehensive discussion of recent improvements made to the inference procedure will be provided by Mason et al, 2022 (in prep). We provide a brief overview but note that the actual inference formalism is identical to that described by (Mason et al., 2019a), aside from the improvements mentioned here. In Figure 2.5, we provide a schematic overview of the entire process, from LBG candidate selection to the final inference of $\overline{x}_{\rm HI}$. Using the Lyα EW and $M_{\rm UV}$ distributions of our three samples of galaxies, we determine the posterior distribution of the global IGM neutral hydrogen fraction, $\overline{x}_{\rm HI}$ at each of the reionization era redshifts, $z \sim 6.7$ and $z \sim 7.6$.

Our analysis uses forward models of the Lyα EW distribution as a function of the average IGM neutral hydrogen fraction $\overline{x}_{\rm HI}$ and galaxies' UV luminosity to infer the evolution of $\overline{x}_{\rm HI}$ as a function of redshift. These forward models are created using reionization simulations from the Evolution of 21cm Structure (EoS) semi-numerical simulations (Mesinger et al., 2016). These simulations generate cubes of the IGM ionization state and dark matter halos during Cosmic Dawn and the EoR using the excursion set principle and include inhomogeneous

recombinations (Sobacchi & Mesinger, 2014). We populate the simulated dark matter halos with $M_{\rm UV}$ values, Lyα line profiles, and EWs based on empirical models derived from our EW values and upper limits (for non-detections) in $z \sim 6.0$ galaxies. $M_{\rm UV}$ values are assigned based on the relationship between halo mass and $M_{\rm UV}$ described by Mason et al. (2015).

We then calculate the observed Lyα EW values over multiple lines of sight after transmission through the IGM. This then provides the likelihood for our observations of each galaxy $p(W \,|\, \overline{x}_{\rm HI}, m, \mu, z_g)$ where W is the Lyα EW, m is the apparent magnitude in the F160W band, μ is the gravitational lensing magnification, and z_g is each galaxy's redshift.

To account for the unknown redshift of our non-detections we use the likelihood of observing a 1D flux density spectrum $\{f\} = f(\lambda_i)$ for an individual galaxy (where i is the wavelength pixel index), given our model where the true EW is drawn from the conditional probability distribution $p(W \,|\, \overline{x}_{\rm HI}, m, \mu, z_g)$:

$$\begin{aligned} &p(\{f\} \,|\, \overline{x}_{\rm HI}, m, \mu, z_g, \mathrm{FWHM}) = \\ &\prod_i^N \int_0^\infty dW \left[\frac{1}{\sqrt{2\pi}\sigma_i} e^{-\frac{1}{2}\left(\frac{f_i - f_{\rm mod}(\lambda_i, W, m, z_d, \mathrm{FWHM})}{\sigma_i}\right)^2} \right. \\ &\qquad \left. \times\, p(W \,|\, \overline{x}_{\rm HI}, m, \mu, z_g) \right] \end{aligned} \tag{2.4}$$

where σ_i is the uncertainty in flux density at wavelength pixel i and there are a total of N wavelength pixels in the spectrum. This product of likelihoods over the wavelength range of the spectrum accounts for the wavelength sensitivity of our observations, i.e., high noise regions are weighted lower than low noise regions.

The posterior distribution for $\overline{x}_{\rm HI}$ is obtained using Bayes' Theorem and after marginalizing over redshift z_g and FWHM for each galaxy. We use a uniform prior on $\overline{x}_{\rm HI}$ between 0 and 1, $p(\overline{x}_{\rm HI})$, a log-normal prior on FWHM with mean depending on $M_{\rm UV}$ as derived by empirical relations and 0.3 dex width (see Appendix C by Mason et al., 2019a) and the photometric redshift distribution for the prior $p(z_g)$. Assuming all observations are independent, the final posterior is the product of the normalised posteriors (Equation 7 by Mason et al., 2019a) for each object.

2.3.2.1 Updates to the Inference Method

A detailed account of all the improvements made to the inference framework since previous analyses (Mason et al., 2018, 2019a; Hoag et al., 2019) will be presented by Mason et al., 2022 (in prep). The major changes are to the determination of the empirical intrinsic (before IGM absorption) Lyα EW distribution, but there are other smaller changes primarily concerned with accounting for all possible sources of error in the inference. However, the general framework, including the population of dark matter halos with Lyα line profiles and EWs, remains the same as that described by Mason et al. (2018, 2019a). The model intrinsic distribution of Lyα EW is now based upon the combination of the De Barros et al. (2017) and Fuller et al. (2020) samples, but the method of using this intrinsic $p(EW)$ to infer $\overline{x}_{\rm HI}$ remains the same. Below we give a brief overview of the improvements relevant to this analysis.

The updates to the inference incorporated in this work fall under two categories: more careful stress testing of galaxies included in the $z \sim 6.0$ reference sample and a more thorough accounting of and propagation of errors throughout the entire process.

Inclusion of the faint LBG sample from this study in the intrinsic Lyα EW model provides a more robust comparison for observations of lensed galaxies at higher redshifts, as we are reducing the amount of factors influencing the differences in Lyα EW distribution between samples at different redshifts (e.g., Mason et al., 2019a; Hoag et al., 2019). Additionally, the data used to determine the empirical EW distribution was more thoroughly tested than in previous iterations of this analysis.

Here we describe several tests we did to check the effect of various treatment of the data on the recovered intrinsic distribution. The sample of $z \sim 6.0$ candidates are those from Fuller et al. (2020) between $5.5 < z < 6.5$. We use two ways to determine which non-emitter candidates are included in this sample: selecting galaxies whose peak $P(z)$ value is between $5.5 < z < 6.5$ and looking at the fraction of integrated $P(z)$ between those redshifts. We find no significant change in the EW distribution parameters by using either the peak $z_{\rm phot}$ or candidates whose total $P(z)$ between $z = 5.5$ and 6.5 is greater than 20%. We also experiment with removing EW data from LAEs flagged as low quality detections by Fuller et al. (2020) from the analysis entirely. Removing these in the determination of

the EW distribution does not significantly change the fit parameters and does not affect our $\overline{x}_{\rm HI}$ inference. Another check we perform is testing whether changes to the error on $M_{\rm UV}$ significantly affect the inference results. Using a minimum $M_{\rm UV}$ error value of 0.3 to account for uncertainties in redshift within the $5.5 < z < 6.5$ range yields no significant change in the posteriors, compared to using $M_{\rm UV}$ errors calculated via uncertainties in the apparent magnitude, most probable redshift, and magnification.

Our updated method also includes propagation of errors in the intrinsic Lyα EW distribution into the final $\overline{x}_{\rm HI}$ posterior. The data we use to determine the EW distribution at $z \sim 6.0$ have inherent uncertainties attached to them, which is now propagated in addition to the previous inclusion of uncertainties in $m_{\rm AB}$, μ, z, line FWHM and line-of-sight variation. The propagation of Lyα EW distribution errors naturally increases the confidence intervals on $\overline{x}_{\rm HI}$: previously, Hoag et al. (2019) inferred a neutral fraction at $z \sim 7.6$ of $\overline{x}_{\rm HI} = 0.88^{+0.05}_{-0.10}$. Running our improved analysis at $z \sim 7.6$ with the same data (only the De Barros et al., 2017 sample as the $z \sim 6.0$ reference sample) yields a $\overline{x}_{\rm HI}$ of $0.83^{+0.09}_{-0.13}$. We note that the small decrease in the inferred median $\overline{x}_{\rm HI}$ value in our work, compared to that published by Hoag et al. (2019), is due to a correction of an error in the intrinsic EW distribution presented by Mason et al. (2018). The $z \sim 7.6$ data used in the inference is identical to that used by Hoag et al. (2019). This error has been corrected in this work. The inclusion of a faint reference sample reduces the confidence interval on $\overline{x}_{\rm HI}$ compared to using the brighter reference sample alone because the intrinsic EW distribution is better constrained at low UV luminosities. This is discussed further below (Section 2.4).

2.4 Results and Discussion

The final results of this work are an inferred upper limit on the neutral fraction at $z \sim 6.7$ of $\overline{x}_{\rm HI} \leq 0.25$ within 68% uncertainty (≤ 0.44 within 95% uncertainty), with the 68% uncertainties derived from error propagation throughout the analysis, and a neutral fraction of $0.83^{+0.08}_{-0.11}$ at $z \sim 7.6$, ($0.83^{+0.11}_{-0.21}$ within 95% uncertainty). The final posteriors can be seen in Figure 2.6. We include the $z \sim 7.6$ posterior derived using both the bright De Barros et al. (2017) reference sample and our faint Fuller et al. (2020) $z \sim 6.0$ sample on top of that computed using only the bright reference sample. The results using only bright galaxies in

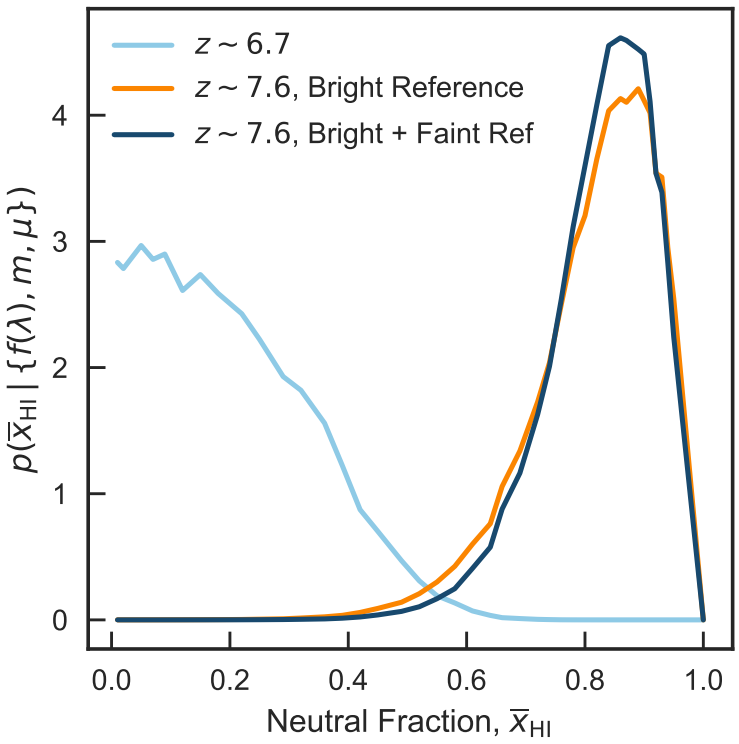

Figure 2.6: Posterior distributions of $\overline{x}_{\rm HI}$ for galaxies at $z \sim 6.7$ (light blue) and at $z \sim 7.6$ (dark blue and orange). At $z \sim 7.6$, we show posteriors for the inferences using only the bright De Barros et al. (2017) $z \sim 6.0$ reference sample (orange) and those made using both the bright and faint Fuller et al. (2020) galaxies (dark blue). By adding in a large sample of faint galaxy candidates, we reduce the uncertainty in our posterior distribution, as the curve derived from this work represents a tighter posterior.

the reference sample yields a $\overline{x}_{\rm HI}$ of $0.83^{+0.09}_{-0.13}$. With our inclusion of a faint reference sample, the inferred neutral fraction is $0.83^{+0.08}_{-0.11}$.

By adding in a large sample of intrinsically faint galaxies at $z \sim 6.0$, we reduce uncertainties in the inference of $\overline{x}_{\rm HI}$ at $z \sim 6.7$ and $z \sim 7.6$ by better constraining the EW distribution of Lyα before transmission through the IGM. Our errors on the neutral fraction at $z \sim 7.6$ reflect a 14% reduction in uncertainty from the Hoag et al. (2019) analysis using the same $z \sim 7.6$ sample. Figure 2.7 shows our two values alongside others derived from a range of methods which employ inhomogeneous models of reionization history. Shaded in grey are the 68 and 95 percent confidence intervals on the reionization history, calculated from Planck Collaboration et al. (2020) CMB optical depth and dark pixel fraction constraints (Mason et al., 2019b). Our two values are consistent within 68% with these constraints.

Our inferred neutral fraction values at $z \sim 6.7$ and $z \sim 7.6$ are consistent with a fairly rapid and late reionization, with close to 50% of hydrogen in the IGM becoming ionized between these two redshifts. A $\overline{x}_{\rm HI}$ of $0.83^{+0.08}_{-0.11}$ at $z \sim 7.6$ implies a universe composed of mostly neutral hydrogen at this redshift, which quickly drops within less than 100 Myrs by $z \sim 6.7$ down to one quarter or less of IGM neutrality. It is likely that young stars within galaxies, perhaps with a contribution from quasars or lower luminosity AGN (see Grazian et al., 2016 and references therein) were emitting bulk amounts of ionizing photons into the IGM in this time period (e.g., Bouwens et al., 2003; Yan, 2004; Finkelstein et al., 2015). It is also possible that the contribution of bright galaxies increases with cosmic time (Smith et al., 2021).

In the discussion which follows, we note that we can only make direct comparisons to studies which include inhomogeneous reionization or account for sightline variance when contextualizing our results with them, as these effects significantly influence the determination of $\overline{x}_{\rm HI}$. We also only include such studies in Figure 2.7.

Our upper limit on the neutral fraction at $z \sim 6.7$ is consistent within other limits placed at similar redshifts. Our upper limit is lower than that found using a group of clustered LAEs at $z \sim 6.6$ (Ouchi et al., 2010; Sobacchi & Mesinger, 2015). By including the information from a full sample of LBG candidates, even those without detected Lyα emission, we are able to place tighter constraints on the neutral fraction. Morales et al. (2021) recently performed similar inferences on $\overline{x}_{\rm HI}$ during reionization using realistic models of the Lyα LF with Lyα EW models to infer neutral fractions, shown as pentagons in Figure 2.7, which are consistent with our two constraints within errors. The evolution of the three values from Morales et al. (2021) also supports a late reionization scenario, assuming the process is complete by $z \sim 6$. The simulations introduced by Kannan et al. (2021) also agree with a relatively fast reionization history, but favor it occurring later in cosmic time.

As we get closer to the end of the EoR, it becomes more difficult to place a lower limit on $\overline{x}_{\rm HI}$ due to intervening remaining patches of neutral hydrogen. Our method assumes reionization is complete at $z \sim 6$. However, this is not found by some recent studies which use opacity fluctuations in the Lyα or Lyβ forests at $5 < z < 6$ (e.g., D'Aloisio et al., 2015; Bosman et al., 2021; Zhu et al., 2021, 2022); these analyses find that the end of reionization

may be later than $z \sim 6$. It is difficult to pinpoint an end to reionization, due to its patchiness. However, the exact point does not significantly influence our results, as the measured $\overline{x}_{\rm HI}$ below $z < 6$ is small (e.g., Morales et al., 2021).

Our $z \sim 7.6$ value agrees with many independent measurements of $\overline{x}_{\rm HI}$ and is in mild tension with a few. A variety of studies probing both quasars and galaxies have found neutral fraction values which agree with ours. The value we find is higher, though not significantly so, than that found using the damping wings of a bright quasar at $z = 7.54$ (Bañados et al., 2018), calculated by Davies et al. (2018): $\overline{x}_{\rm HI} = 0.56^{+0.21}_{-0.18}$. Recent findings from the SILVERRUSH team (Ouchi et al., 2018) use the Lyα LF to constrain the neutral fraction at $z \sim 7.6$ to be greater than 0.28 (Goto et al., 2021), consistent with the project's previous result of $\overline{x}_{\rm HI} = 0.5^{+0.1}_{-0.3}$ at $z = 7.3$ (Inoue et al., 2018). Wold et al. (2022) place an upper limit on the neutral fraction at $z = 6.9$ of 0.33. All of these results are in agreement with our two values, although it is difficult to make a direct comparison, as the inhomogeneity of reionization is not taken into account. The higher precision on our values reflects the use multiple lines of sight with galaxies in a range of environments, which alleviates cosmic variance (Mason et al., 2018; Whitler et al., 2020).

In contrast, there are a few studies whose $\overline{x}_{\rm HI}$ values do not agree with ours within $\sim 1\sigma$. Greig et al. (2019) find a $\overline{x}_{\rm HI}$ of $0.21^{+0.17}_{-0.19}$ at $z = 7.54$ using the same quasar presented by Bañados et al. (2018), with a significantly different result from Davies et al. (2018) due to a different intrinsic Lyα emission model. Jung et al. (2020) calculate a $\overline{x}_{\rm HI}$ value of $0.49^{+0.19}_{-0.19}$ at $z \sim 7.6$, a difference of $\sim 1.5\sigma$ from our result, using Lyα emission from 10 galaxies at $z > 7$ but do not take the inhomogeneous nature of reionization into account. Notably, these works, unlike our own, do not use faint ($< L^*$) galaxies when determining the neutral fraction, and it is these galaxies which may be producing the majority of ionizing photons (Bouwens et al., 2015; Finkelstein et al., 2015; Livermore et al., 2017). Faint galaxies are also in the least biased environments on average as evidenced by clustering measurements (e.g., Durkalec et al., 2018). Other probes of reionization, such as quasars and bright LBGs, investigate denser and possibly biased regions surrounding high-mass halos with bright luminosities which may not be representative of a typical region during reionization (Ouchi et al., 2005; Orsi et al., 2016; Durkalec et al., 2018). Our inclusion of faint galaxies gives a

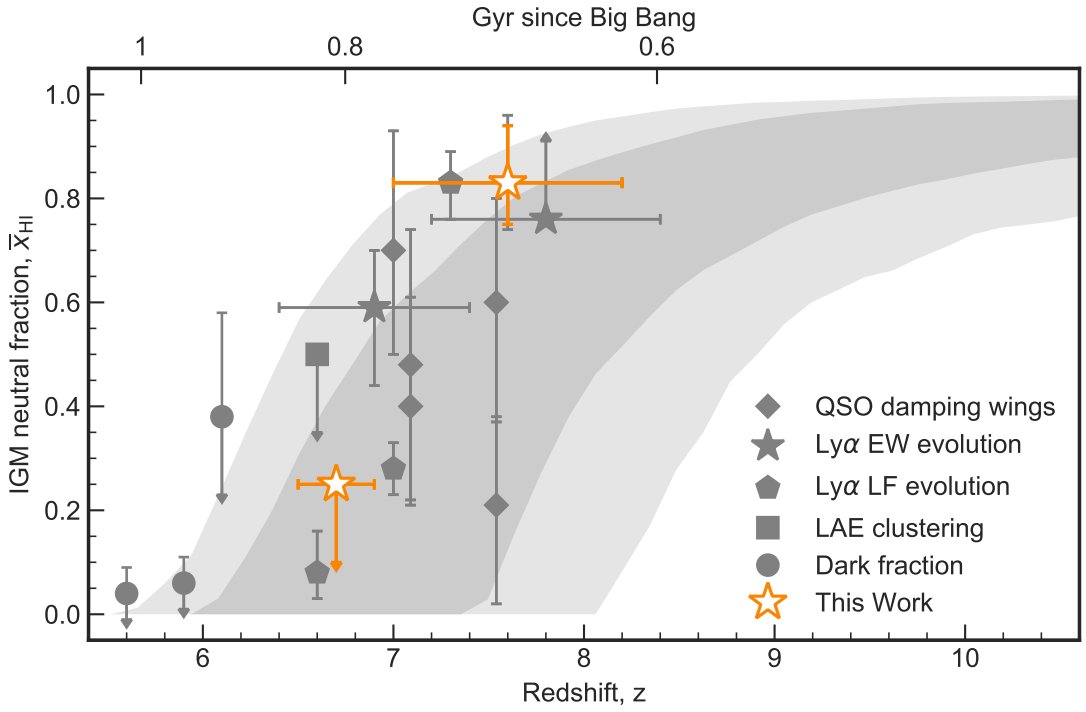

Figure 2.7: New measurements of $\overline{x}_{\rm HI}$ (orange stars) compared to values derived from other studies. All error bars and upper limits correspond to 1σ. The 68 and 95 percent confidence intervals on the reionization history are shaded in grey, calculated from Planck Collaboration et al. (2016) CMB optical depth and dark pixel fraction constraints (Mason et al., 2019b). The grey stars represent inferred $\overline{x}_{\rm HI}$ values using the same Bayesian analysis as this work (Mason et al., 2018, 2019a; Hoag et al., 2019). Note the point from the previous analysis (Hoag et al., 2019) at the same point as this work but with larger error bars. Other data points are from a related inference method which incorporates the evolution of the Lyα luminosity function (Morales et al., 2021), the clustering of LAEs as squares (Ouchi et al., 2010; Sobacchi & Mesinger, 2015), Lyα and Lyβ forest dark pixel fraction in circles (McGreer et al., 2015), and diamonds representing quasar damping wings (Davies et al., 2018; Greig et al., 2019; Wang et al., 2020).

more accurate picture of reionization because we can trace reionization over a very broad range of environments, not just the most overdense regions where bright galaxies reside. The combined constraints on the neutral fraction from galaxies across a range of magnitudes increases the precision of our measurement (Whitler et al., 2020). Endsley et al. (2021) also find a decline in intrinsic Lyα EW strength from $z \sim 7$ to $z \sim 6$ in their bright galaxy sample, but with less contrast than we find in our faint samples. This supports the scenario where bright galaxies reside in overdensities which reionize early (e.g., Mason et al., 2018; Qin et al., 2022).

Our $\overline{x}_{\rm HI}$ value is one of several at $z > 7$ (e.g., Davies et al., 2018; Greig et al., 2019; Hoag

et al., 2019; Jung et al., 2020; Wang et al., 2020; Morales et al., 2021). In order to determine a detailed timeline of reionization history, observations of large samples of galaxies at high redshift are imperative. Surveys similar to the ones used in this work at $z \sim$ 7-10 will become more readily available with the launch of *JWST*. Using a combination of NIRCAM photometric data and spectroscopy from the NIRSPEC or NIRISS instruments, we will be able to do studies similar to this one on large samples of faint LBGs at $z \geq 8$.

While there is no change in the recovered inferred neutral hydrogen fraction of the IGM at $z \sim 7.6$ in our updated method as compared to a previous attempt, there are clear improvements to using a galaxy population which has similar characteristics to the $z \sim 6.7$ and $z \sim 7.6$ galaxies that allow us to better characterize several parts of this analysis. These improvements will prove even more important for future larger samples of LBGs. The consistency in $\overline{x}_{\rm HI}$ between the previous approach and our updated analysis speaks to the robustness of the inference method. By introducing a large sample of low-luminosity galaxy candidates to the inference method, the EW distribution in the ionized universe can be more tightly constrained, leading to a smaller uncertainty in the final posterior.

2.5 Conclusions

We have combined a lensed, intrinsically faint sample of nearly 200 LBG candidates (Fuller et al., 2020) with 68 low-luminosity candidates at $z \sim 7.6$ (Hoag et al., 2019) for use in a Bayesian framework developed by Mason et al. (2018, 2019a) in order to constrain the global IGM neutral fraction, $\overline{x}_{\rm HI}$, at $z \sim 6.7$ and $z \sim 7.6$. This work expands upon that done in Mason et al. (2018) and Hoag et al. (2019) by adding a large, faint population of galaxies to the De Barros et al. (2017) reference sample at $z \sim 6.0$, as well as folding in a more thorough analysis of the various uncertainties and assumptions inherent in this method. A summary of our conclusions is as follows:

- We find no significant evidence of a difference between the faint $z \sim 6.0$ reference sample and those of the two higher redshift samples based on β slope and $M_{\rm UV}$. This result comes from comparing the UV β slope and the $M_{\rm UV}$ distributions of the three samples using a Monte Carlo method to account for uncertainties in the $P(z)$ distributions for individual LBG candidates.

- Inclusion of the Fuller et al. (2020) sample of $z \sim 6.0$ galaxies yields the same neutral fraction at $z \sim 7.6$ as the analysis using only the De Barros et al. (2017) sample at $z \sim 6.0$, but with a 14% reduction in uncertainty. In this work, we infer a $\overline{x}_{\rm HI}$ of $0.83^{+0.08}_{-0.11}$ ($0.83^{+0.11}_{-0.21}$), at the 1 σ (2 σ) level compared to $\overline{x}_{\rm HI} = 0.83^{+0.09}_{-0.13}$ at the 1 σ level without using the faint sample.

- We place an upper limit on $\overline{x}_{\rm HI}$ at $z \sim 6.7$ of 0.25 within 68 % uncertainty and 0.44 within 95 % uncertainty. These two results are consistent with other studies at similar redshifts (Planck Collaboration et al., 2020; Davies et al., 2018; Mason et al., 2019b; Hoag et al., 2019; Morales et al., 2021), are at mild tension with others (Greig et al., 2019), and imply fairly rapid reionization.

- Incorporating low-luminosity galaxies yields a higher precision on the neutral fraction at $z \sim 7.6$ than other studies at similar redshift. We are probing typical galaxies during the EoR, as faint galaxies exist in much higher numbers than their bright counterparts. Our $\overline{x}_{\rm HI}$ reflects a globally-averaged neutral fraction derived from multiple sightlines.

Over the next few years, we plan to take follow-up spectroscopic observations with Keck, *JWST*, and ALMA, to target other nebular emission lines such as [CII] and CIII] in the LBG candidates in these datasets. Once precise redshifts are conclusively determined, the statistical power of this work will dramatically improve by removing impurities and no longer requiring cuts on the integrated $P(z)$. With future larger samples, especially at $z \geq 7$, this method is promising for the measurement of $\overline{x}_{\rm HI}$ over many EoR redshifts to constrain a detailed timeline of cosmic history during reionization.

Acknowledgements

We thank the anonymous referee for their comments and suggestions. This material is based upon work supported by the National Science Foundation under Grant No. AST-1815458 to M.B. and grant AST1810822 to T.T., and by NASA through grant NNX14AN73H to M.B. C.M. acknowledges support provided by NASA through the NASA Hubble Fellowship grant HST-HF2-51413.001-A awarded by the Space Telescope Science Institute, which is operated by the Association of Universities for Research in Astronomy, Inc., for NASA, under contract

NAS5-26555, and by VILLUM FONDEN through research grant 37459. MB also acknowledges support by the Slovenian national research agency ARRS through grant N1-0238. Based on spectrographic data obtained at the W.M.Keck Observatory, which is operated as a scientific partnership among the California Institute of Technology, the University of California, and the National Aeronautics and Space Administration. The Observatory was made possible by the generous financial support of the W.M. Keck Foundation. We thank the indigenous Hawaiian community for allowing us to be guests on their sacred mountain, a privilege, without which, this work would not have been possible. We are most fortunate to be able to conduct observations from this site. Also based on observations made with the NASA/ESA Hubble Space Telescope, obtained at the Space Telescope Science Institute, which is operated by the Association of Universities for Research in Astronomy, Inc., under NASA contract NAS5-26555. And based on observations made with the Spitzer Space Telescope, which is operated by the Jet Propulsion Laboratory, California Institute of Technology under a contract with NASA. Support for this work was also provided by NASA/HST grant HST-GO-14096, and through an award issued by JPL/Caltech.

This work used the following software packages: AstroPy (The Astropy Collaboration et al., 2018), SExtractor (Bertin & Arnouts, 1996), iPython (Perez & Granger, 2007), Matplotlib (Hunter, 2007), and NumPy (van der Walt et al., 2011).

Data Availability

All characteristics for the $z \sim 7.6$ galaxies are presented in Table 5 by Hoag et al. (2019), and those of the LAEs from the DEIMOS sample are summarized in Table 3 by Fuller et al. (2020). Data describing the non-emitters from Fuller et al. (2020) are summarized in a table uploaded to CDS.

Chapter 3

Lyα Emission Strength and Stellar Properties Among Typical Galaxies from $5 < z < 8.2$

This chapter has been submitted to *MNRAS* as of September 29, 2023 and is currently under review.

We present a study on stellar properties of Lyman-alpha (Lyα) emitters at $5 < z < 8.2$. We use 247 photometrically-selected, lensed, high-redshift, low luminosity galaxy candidates with spectroscopic follow-up. Of these, 38 are confirmed spectroscopically to be between $5 < z < 8.2$ via detection of Lyα. For each galaxy and candidate, we estimate stellar mass, star formation rate, specific star formation rate, and mass-weighted age with spectral energy density fitting. We also measure the UV β slope and luminosity using values from photometry. We find no strong correlation between Lyα equivalent width and any of these properties, as well as no significant difference between the physical properties of Lyα emitters and candidates without Lyα detected. This lack of expected trends may be explained by a combination of the evolving opacity of the IGM at these redshifts as well as the unique phase space probed by our lensed sample. Via tests on other galaxy samples which show varying strengths of correlations, we conclude that if there exist any relationships between Lyα EW and physical properties in the underlying population of faint galaxies, they are weak correlations. We also present the results of a spectroscopic search for CIII] emission

in confirmed Lyα emitters at $z \sim 7$, finding no CIII] detections, but putting constraints on strong AGN activity and extreme nebular emission.

galaxies: evolution – galaxies: high-redshift – dark ages, reionization, first stars

3.1 Introduction

There are still many open questions about the Epoch of Reionization (EoR) surrounding the responsible sources and the detailed mechanisms of how it occurred. Observations of high redshift ($z > 6$) galaxies are critical to answer many of these questions. Through extensive observational studies over the past decades, galaxies have been identified as likely playing a dominant role in reionization relative to other sources such as quasars (e.g. Bouwens et al., 2015; Finkelstein et al., 2019a; Robertson, 2021; **?**; Fan et al., 2023; Robertson et al., 2023). However, it still remains unclear whether massive and bright galaxies emitted the majority of ionizing photons coming from galaxies (e.g. Robertson et al., 2015; Naidu et al., 2020; Lin et al., 2023) or the ionizing budget was dominated by fainter, yet more numerous galaxies (e.g. Finkelstein et al., 2019b; Mascia et al., 2023a).

Determining the characteristics of galaxies in the EoR through observations is crucial to constraining the relative contribution to reionization of bright and faint galaxies. With substantial samples of EoR galaxies, we can estimate physical properties and correlate those with some measure of how efficient the galaxies are at ionizing. The metric needed to determine this efficiency is the rate of Lyman continuum (LyC) escape from these galaxies, $f_{\rm esc}$. However, this value is not directly attainable due to the opacity of the intergalactic medium (IGM) at these redshifts. Indirect estimations and correlations with measurable properties are possible, however. Surveys of galaxies at lower redshifts reveal a correlation between the strength of Lyman-alpha emission (Lyα, 1216 Å) and the escape of LyC photons into the IGM (Pahl et al., 2021; Flury et al., 2022; Begley et al., 2022; Saldana-Lopez et al., 2023). Therefore, we use Lyα emission as a proxy for ionizing photon production in order to begin to characterize a typical galaxy that had a dominant role in reionizing the IGM.

Lyα is a powerful probe of galaxies in the EoR as it is intrinsically the strongest line in the UV. However, Lyα photons are scattered by neutral hydrogen, making the line a probe of the ionization state of the IGM as well as properties of the sources that emitted

them (e.g. **?**Treu et al., 2012; Dijkstra, 2014). Analyzing the physical properties of Lyα emitters (LAEs) during the EoR, how they correlate with Lyα strength, and how they differ from the general population of galaxies for which Lyα emission is not detected, provides a pathway to revealing the mechanisms behind the galaxies that likely powered reionization. If there is evidence of enhanced Lyα emission from galaxies with certain physical properties, it may be possible to distinguish which ones dominated the output of ionizing photons during reionization.

In the past few decades, there have been increasingly more high redshift LAEs detected. With the Hubble Space Telescope (*HST*) and *Spitzer* space telescope, space-based photometry has unveiled many candidates high-redshift Lyman Break Galaxies (LBGs) based on multiband observations (e.g. Stark et al., 2010; Huang et al., 2016a). Follow-up spectroscopy of these candidates has yielded samples of confirmed LAEs. Since the successful launch and deployment of the James Webb Space Telescope (*JWST*), many more LAEs at $z > 6$ are being identified (e.g. Jung et al., 2023; Witstok et al., 2023; Scholtz et al., 2023; Jones et al., 2023a; Saxena et al., 2023b,a; Tang et al., 2023; Maseda et al., 2023; Iani et al., 2023; Bunker et al., 2023). However, while high redshift galaxies are being unveiled back to the first few hundred million years after the Big Bang, large samples of galaxies during the heart and tail end of the EoR remain extremely useful to help characterize the drivers of reionization, especially as it is difficult to detect low equivalent width LAEs using the NIRSpec prism. Until there are substantial samples of EoR galaxies with spectroscopy from *JWST* between $5 < z < 8$, we can gain valuable insights from the collections of galaxies with ground based spectroscopic observations available now.

In this work, we use a sample of 247 lensed $z \sim 5-8.2$ LBG candidates from Fuller et al. (2020) and Hoag et al. (2019), 38 of them with Lyα detected in emission. This is the largest faint ($L \sim 0.1L^*$ where L^* is the characteristic luminosity) sample at this redshift, assembled from hundreds of orbits on *HST*, *Spitzer*, and an over six-year long campaign on the Keck DEep Imaging Multi-Object Spectrograph (DEIMOS; Faber et al., 2003) and Multi-Object Spectrometer For Infra-Red Exploration (MOSFIRE; McLean et al., 2010). We estimate and compute various physical properties of the LBG candidates and spectroscopically confirmed LAEs: UV β slope, UV luminosity, stellar mass, star formation rate (SFR), specific star

formation rate (sSFR), and mass-weighted age. In order to determine if there are significant physical differences in populations of LAEs vs nonLAEs[1], we compare these properties of both samples in bulk. For the LAEs, we look at the strength of the Lyα emission, via both equivalent width (EW) and line luminosity, versus each estimated physical property to see if there are statistically significant trends that may help predict both the presence and strength of Lyα in these galaxies. Past surveys of LAEs and LBGs with this sample size typically probe luminosites of the order L^* and do not extend higher than $z \sim 6$ (e.g. Pentericci et al., 2009; Stark et al., 2010; Oyarzún et al., 2017; Santos et al., 2020). Due to gravitational lensing, our sample extends down to luminosites of $0.001L^*$, making this work unique in its characterization of faint EoR galaxies.

The paper is organized as follows. In Section 2, we discuss the data and observations which comprise this sample. In section 3, we present the methodology of the galaxy property estimation and measurement process used in this study. Section 4 describes the analysis of potential correlations between Lyα emission strength and physical properties of galaxies with spectroscopic confirmation of Lyα. Section 5 covers a comparison of LAEs and the nonLAE sample. In section 6, we present a study of spectral properties in a subsample of LAEs at $z \sim 7$. In Section 7, we present and discuss our results, and conclusions can be found in Section 8. Whenever needed, we use ΛCDM cosmology with $\Omega_m = 0.3, \Omega_\Lambda = 0.7, H_0 = 70$. All magnitudes are given in the AB system (Oke & Gunn, 1983), and all EWs are presented in the rest frame with a positive value indicating emission.

3.2 Data and Observations

The sample used in this study is comprised of 247 Lyman Break galaxies candidates selected using the dropout method with photometry from *HST* and *Spitzer*. Each candidate is followed up with a spectroscopic search for Lyα, 64 of them on Keck/MOSFIRE, and 198 on Keck/DEIMOS, with 15 of these observed with both instruments.

The data used in this analysis come from two sets of observations: a sample of galaxy candidates between $z \sim 5-7$ (Fuller et al., 2020), and another set between $z \sim 7-8.2$ (Hoag

[1]Throughout the paper, this term will refer to LBG candidates with sufficiently constraining spectroscopic limits to rule out Lyα in emission at a level of EW(Lyα)¡25Å, which is the Lyα strength we use to delineate LAEs from non-emitters in this work.

et al., 2019). The candidates are detected behind massive lensing clusters. Each target LBG has photometric measurements from some combination of the following: *HST* Advanced Camera for Surveys (ACS; Ford et al., 1998) and Wide Field Camera (WFC3; Kimble et al., 2008) filters: F435W, F475W, F555W, F606W, F625W, F775W, F850LP, F814W, F105W, F110W, F125W, F140W, and F160W. Five of the clusters are from Hubble Frontier Fields (HFF, Lotz et al., 2017): A2744, MACS0416, MACS0717, MACS1149, and A370. Four clusters come from the Cluster Lensing and Supernova Survey with Hubble (CLASH, Postman et al., 2012), MACS0744, MACS1423, MACS2129, and RXJ1347, and the last, MACS2214, has *HST* imaging from the Spitzer UltRa Faint SUrvey Program (SURFSUP, Bradač et al., 2014). In addition to *HST* imaging from these programs, each cluster has *Spitzer* observations from SURFSUP and the *Spitzer* HFF programs from the 3.6μm and 4.5μm channels on the Infrared Array Camera (IRAC; Fazio et al., 2004). A summary of the cluster fields in this sample is given in Table 3.1.

The original photometric sample from which the smaller spectroscopic sample was chosen was selected by the Lyman Break technique, as mentioned above. To choose the candidates included in this work, we use constraints on the photometric redshift and probability of redshift distribution, or $P(z)$. These $P(z)$s are determined using Easy and Accurate Redshifts from Yale (EAzY; Brammer et al., 2008). This process is described in detail in Huang et al. (2016b) and Strait et al. (2020). Briefly, the code performs χ^2 minimization over a grid of redshifts and computes the $P(z)$ distribution assuming a flat prior due to the candidates being lensed. The sample of candidate LAEs to be followed up spectroscopically was selected following the methods of Hoag et al. (2019) and Fuller et al. (2020).

3.2.1 Photometry

The photometric measurements for the candidates in the cluster fields of A2744, A370, MACS0416, MACS0717, and MACS1149 are from the ASTRODEEP team (Castellano et al., 2016; Di Criscienzo et al., 2017; Bradač et al., 2019). For the remaining clusters, we use an identical method to that employed by the ASTRODEEP team for photometric measurements. Briefly, point-spread function (PSF) matched HST images were created, in which all of the HST images had their PSF degraded to match that of the F160W images. The F160W

Summary of Observations

Cluster Name	Short Name	α_{J2000} (deg)	δ_{J2000} (deg)	$z_{\rm cluster}$	# of candidates	# of Lyα detections	*HST* Imaging (*Spitzer* Imaging)
Abell 2744	A2744	3.5975000	-30.39056	0.308	25	1	HFF
Abell 370	A370	39.968000	-1.576666	0.375	28	3	HFF
MACSJ0416.1-2403	MACS0416	64.039167	-24.06778	0.420	21	3	HFF/CLASH
MACSJ0717.5+0745	MACS0717	109.38167	37.755000	0.548	10	5	HFF/CLASH (SURFSUP)
MACSJ0744.8+3927	MACS0744	116.215833	39.459167	0.686	24	3	CLASH (SURFSUP)
MACSJ1149.5+2223	MACS1149	177.392917	22.395000	0.544	27	2	HFF/CLASH (SURFSUP)
MACSJ1423.8+2404	MACS1423	215.951250	24.079722	0.545	28	6	CLASH (SURFSUP)
MACSJ2129.4-0741	MACS2129	322.359208	-7.690611	0.568	30	5	CLASH (SURFSUP)
MACSJ2214.9-1359	MACS2214	333.739208	-14.00300	0.500	11	1	SURFSUP
RXJ1347.5-1145	RXJ1347	206.87750	-11.75278	0.451	43	9	CLASH (SURFSUP)

Table 3.1: Summary of observations for 10 lensing clusters used in this work.

image was used as the detection band for all fields. In order to improve the detection of faint objects, intracluster light (ICL) was subtracted for targets in each cluster field except for MACS0744 and MACS2214. In these two fields, the ICl subtraction was not performed because the high-redshift objects in these clusters were not heavily contaminated by the ICL. HST photometry was then measured using Source Extractor (SExtractor; Bertin & Arnouts, 1996) in dual-image mode with F160W as the detection image. Photometry for *Spitzer* images was extracted using T-PHOT (Merlin et al., 2015). Further details on this process can be found in Huang et al. (2016a) and Fuller et al. (2020).

3.2.2 Spectroscopy

Out of 247 LBGs, 38 are confirmed LAEs, presented in Fuller et al. (2020); Hoag et al. (2019). To select the final sample used in this work, an inclusive cut of at least 1% of the total integrated probability density of the redshift, $P(z)$, lying in the redshift range where Lyα could be detected on the given instrument with the given setup is used. All analyses done using LBG candidates in this paper are weighted according to amount of the $P(z)$ distribution which lies in this range for a given instrument. This process is described further in section 3.3.3. The spectroscopic observations were made between 2013 and 2017. The average 3σ observed flux limit for the nonemitters is $\sim 2 \times 10^{-18}$ erg/s/cm^2, providing deep constraints on Lyα EW for those targets which did not have detected emission lines. More details on the observations specifics and conditions can be found in Hoag et al. (2019) and Fuller et al. (2020).

As the targets in this survey are gravitationally lensed, determination of magnification, or μ, values were determined for each candidate which we observe. The lens models used are described by **?**Bradač et al. (2009), with details on models for each individual cluster described in Section 3.2 of Hoag et al. (2019). Magnification values for each LBG are determined using the photometric redshift, position, and the generated best-fit magnification map (e.g. **??**). Over the entire sample, magnification values span three orders of magnitude, from ~ 1 to ~ 200.

3.3 Methods

There are six physical properties beyond Lyα emission which we focus on for this study; two are determined directly from the photometry without the use of models other than those used to determine the photometric redshift ($z_{\rm phot}$): UV β-slope and UV luminosity. The remaining four properties are estimated using spectral energy density (SED) fitting: stellar mass, star formation rate, specific star formation rate, and mass-weighted age. For each of these properties, we look at differences between LAEs and nonLAEs, as well as how these properties correlate with Lyα strength for those targets with spectroscopic detections.

3.3.1 Lyα EW

For the 38 galaxies with Lyα detections in the sample, we use the EW values, or relative strength of the Lyα emission line compared to the continuum of the galaxy. What constitutes a detection, as well as the calculation of Lyα EW values, are described by Hoag et al. (2019) and Fuller et al. (2020). While we do not detect emission in the majority of our sample, we are still able to constrain the upper 1σ limit on Lyα EW via

$$\mathrm{EW}_{lim} = \frac{f_{\rm lim}(\lambda)}{f_{\rm cont}(1+z)} \tag{3.1}$$

where the continuum flux density, $f_{\rm cont}$, is defined as

$$f_{\rm cont} = 10^{-0.4(m_{\rm AB}+48.6)} c/\lambda^2$$

erg/s/cm^2/Å(3.2) computed using continuum flux redward of the expected Lyα line, using the following HST bands for $m_{\rm AB}$. For galaxies observed by DEIMOS at $5 < z < 7$, we typically use the apparent magnitude in the F105W band, which corresponds to an average rest-frame wavelength of $\lambda \sim 1500$ Å. If there is no F105W data available, F125W (rest-frame $\lambda \sim 1800$ Å) is used, and, in a few cases, where there is neither an F105W nor F125W magnitude, F140W (rest-frame $\lambda \sim 2000$ Å) is used. For those observed with MOSFIRE between $7 < z < 8.2$, we use the F160W band. The quantity $f_{\rm lim}$ is the flux density value of the 1σ noise spectrum at the expected spectral location of the emission line. We note that gravitational lensing is achromatic, and therefore EW is invariant with respect to magnification value.

3.3.2 UV Property Calculations

Two UV properties of the galaxies in our sample can be calculated via photometric fluxes: the UV β slope and UV luminosity. The UV continuum slope of a galaxy's spectrum, or its β slope, characterizes its flux redward of Lyα emission with the relation $f_\lambda \propto \lambda^\beta$. The steepness of the β slope can give insight into stellar populations and the degree of dust reddening in a galaxy (Buat et al., 2012; Yamanaka & Yamada, 2019; Calabrò et al., 2021; Chisholm et al., 2022). We compute the β slope for each LBG candidate that has the requisite data as set by the following. We require at least two magnitude measurements in filters redward of the expected Lyα emission. All β slopes are calculated in the observed frame using linear regression fitting of the uncertainty-weighted magnitude values against the effective wavelength of the filter from *Scikit-Learn* (Pedregosa et al., 2018).

The intrinsic UV luminosity, or $M_{\rm UV}$, is calculated via

$$M_{\rm UV} \approx M_{\rm FUV} = m_{F160W} + 2.5\log_{10}(\mu) - 5(\log_{10}(d_L) - 1) + 2.5\log_{10}(1+z) + 0.12 \quad (3.3)$$

where m_{F160W} is the apparent magnitude in the F160W band, μ is the median magnification value recovered from lens modelling, d_L is luminosity distance in parsecs, z is the redshift, and 0.12 is a K-correction to correct to rest frame 1600Å (see Fuller et al., 2020 for details).

3.3.3 Estimating Galaxy Properties

To estimate stellar properties of the sample, we use Bayesian Analysis of Galaxies for Physical Inference and Parameter EStimation (BAGPIPES, Carnall et al., 2018). BAGPIPES fits physical parameters using the MultiNest sampling algorithm (Feroz & Hobson, 2008; Feroz et al., 2009). We use the default set of stellar population templates from Bruzal and Charlot (Bruzual & Charlot, 2003, BC03). The SED fitting is done using the initial mass function (IMF) from Kroupa & Boily (2002), a metallicity of $0.02Z_\odot$, a Calzetti dust law (Calzetti et al., 2000), and a constant star formation history (SFH).We allow dust extinction to range from A_v = 0-3 magnitudes. When we allow metallicity to vary between 0-2$Z_\odot$, our median best fit value is $0.03Z_\odot$, agreeing with other sets of observations and simulations (Seeyave et al., 2023; Dekel et al., 2023), and we find no significant difference in the resultant posteriors whether we fix at $0.02Z_\odot$ or allow it to vary. We perform parallel runs employing

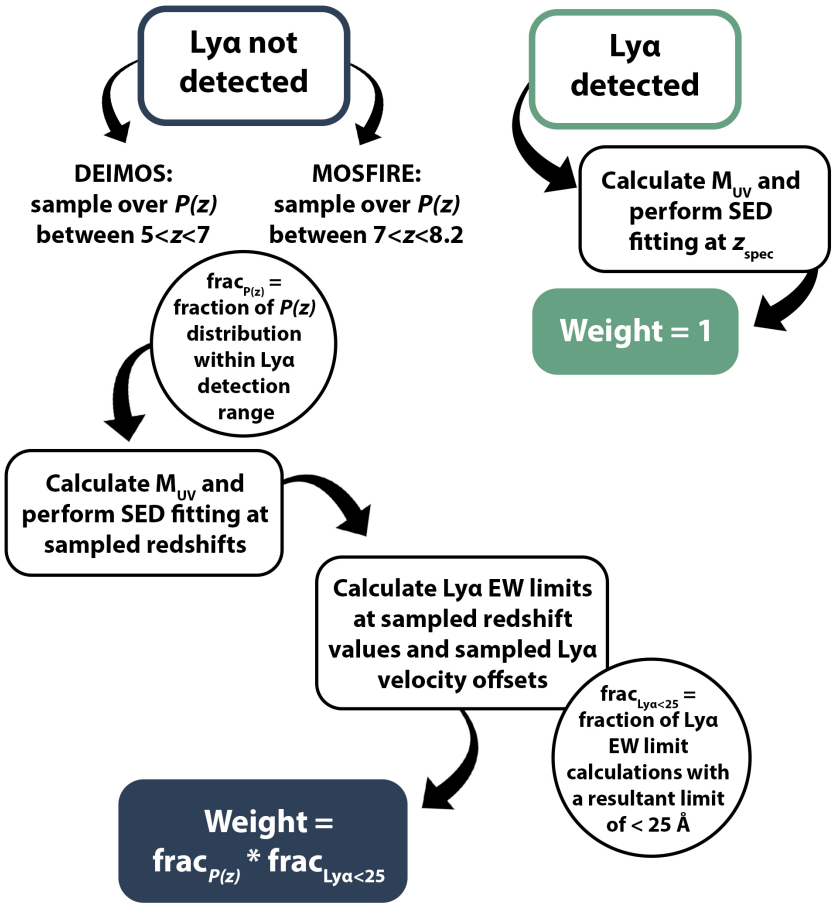

Figure 3.1: Schematic diagram explaining the process used to determine weights used in the analysis, incorporating both the fraction of the $P(z)$ distribution which lies within the Lyα detection range and the fraction of EW limit calculations which are $\leq$ 25Å at the 3σ level. This method allows us to take into account the uncertainties in redshift for nonLAEs.

a delayed tau SFH and find that it has no effect on our conclusions. We also run the fits using different dust laws - Cardelli, CF00 (Charlot & Fall, 2000), and Salim (Salim et al., 2018) - and find no significant difference in the resultant estimated parameters. For each SED run, we input a redshift value to fit at. For targets with Lyα detections, the redshift is fixed either at the spectroscopic redshift or, in the case of nonLAEs, the redshift sampled from the $P(z)$ for a given Monte Carlo (MC) iteration through a process we describe in the next section.

3.3.4 Monte Carlo Processes and Weighting Scheme

The determination of all of these physical properties relies on the input of a redshift value for the galaxy in question; parameters estimated from SED fitting, $M_{\rm UV}$, β slope, and Lyα

EW limit all have dependence on z. To determine these values for LBGs which do not have a confirmed spectroscopic redshift, we use an MC sampling method in order to properly treat the uncertainty in redshift. Figure 3.1 provides a schematic diagram of the MC processes and how they are used to determine appropriate weights for properties of nonemitters when comparing their properties to LAEs. We give detailed descriptions of these processes below.

In comparing properties of LAEs against those of nonLAEs, we create a weighting system which takes into account the uncertainty in redshift and how that propagates to uncertainties in SED-derived properties and Lyα EW measurements. For physical properties, we sample over the part of the $P(z)$ distribution which is in the range of possible Lyα detection. For DEIMOS targets, the Lyα line is potentially visible for targets between $5 < z < 7$, and for those with spectroscopy from MOSFIRE, between $7 < z < 8.2$. After sampling a distribution of z values from each target's $P(z)$, we run the SED fit at the sampled redshifts and produce distributions of physical properties for each of the nonemitters. When we compare these properties for LAEs against nonemitters, we include the full distribution of output parameters for each galaxy, with each value weighted as described below.

As the flux limits from our detections are wavelength dependent, the redshift also affects the determination of Lyα EW from the expected spectral location of the emission line. We once again sample redshifts from the $P(z)$ in the desired redshift range. We then sample from the distribution of Lyα-ISM velocity offsets (Δv) from Cassata et al. (2020), as Lyα emission is often spectrally offset from the systemic redshift of a galaxy. For a chosen redshift, we determine the spectral location of Lyα, apply the offset sampled from the Lyα Δv distribution, and choose the value in the flux density spectrum at that wavelength. We then calculate the 1σ Lyα EW upper limit using Eq. 3.1 and multiply it by 3 to obtain 3σ upper limits.

When comparing properties of LAEs and nonLAEs, we use the fiducial cutoff of $\mathrm{EW}_{\mathrm{Ly}\alpha} <$ 25Å to determine non-LAEs (e.g. Mason et al., 2018; Pentericci et al., 2018). Once we obtain a distribution of output parameters from the SED fitting as well as one of measured Lyα EW limits for each nonemitter, we create a weight for each one based on how likely they are to be in the the desired redshift range and have an EW limit ¡ 25Å. The nonemitter sample is weighted by the product of the fraction of EW determinations runs for which Lyα EW

is $<$ 25 Å and the fraction of total integrated $P(z)$ which is in the desired range for the given spectroscopic instrument. As each nonemitter has a distribution of 100 values for the properties estimated from SED fitting, each of those values receives a weight of 1/100th of that of the total weight for the galaxy. As an example, if a candidate has a $P(z)$ distribution with of its When comparing properties of LAEs and nonLAEs, we use the fiducial cutoff of $\mathrm{EW_{Ly\alpha}} < 25$Å to determine non-LAEs (e.g. Mason et al., 2018; Pentericci et al., 2018). Once we obtain a distribution of output parameters from the SED fitting as well as one of measured Lyα EW limits for each nonemitter, we create a weight for each one based on how likely they are to be in the the desired redshift range and have an EW limit ¡ 25Å. The nonemitter sample is weighted by the product of the fraction of EW determinations runs for which Lyα EW is $<$ 25 Å and the fraction of total integrated $P(z)$ which is in the desired range for the given spectroscopic instrument. As each nonemitter has a distribution of 100 values for the properties estimated from SED fitting, each of those values receives a weight of 1/100th of that of the total weight for the galaxy. As an example, if a candidate observed with DEIMOS has 40% of its $P(z)$ distribution within $5 < z < 7$ and 80% of the Lyα EW limit calculations below a 3σ limit of 25Å then each individual realization of that galaxy's properties would have a weight of $0.4 * 0.8/100 = 0.0032$, and that galaxy's total contribution to the distribution would have a weight of 0.32.

3.4 Lyα EW vs Physical Properties

For the 38 galaxies which have spectroscopic Lyα detections, we use the EW values calculated by Hoag et al. (2019) and Fuller et al. (2020) and see if there are trends between a galaxy's Lyα EW and the following physical properties: stellar mass, SFR, sSFR, mass-weighted age, UV β slope, and M_{UV}. We also perform the same analysis with delensed Lyα line luminosity rather than EW and recover the same results for all properties except M_{UV}, an exception we discuss in section 3.4.1.

There have been many studies looking at these correlations at $2 \leq z \leq 7$ (e.g., Pentericci et al., 2009; Kornei et al., 2010; Nilsson et al., 2011; Hathi et al., 2016; Oyarzún et al., 2017; Du et al., 2018; Marchi et al., 2019; Santos et al., 2020; Pucha et al., 2022; McCarron et al., 2022; Reddy et al., 2022; Napolitano et al., 2023; Ortiz et al., 2023; Saldana-Lopez

et al., 2023; Jones et al., 2023a). The outcomes of these studies are varied and show a range of different, sometimes conflicting, trends, depending on the property being studied. In the following sections, we present the results of our work and discuss how they compare to others. We perform Spearman rank tests to quantify any correlations between each of these properties and the Lyα EW. One outcome parameter of the test is a ρ value which ranges from -1 to 1 and quantifies the strength of the correlation, with -1 and 1 designating monotonic anticorrelation and correlation, respectively. The p-value gives a measure of the significance of the correlation, with a value less than 0.005 indicating a correlation at $\geq 3\sigma$ significance. Figure 3.2 shows the Lyα EW vs each of these physical properties along with the results from the corresponding correlation test. Below we present the results of our study; discussions on how they vary from other surveys and potential reasons why can be found in section 3.7.

3.4.1 UV Properties

We first look at Lyα EW vs β slope (see bottom right panel of Figure 3.2), finding no significant relationship. From previous studies and galactic physics, we may expect that larger Lyα EW would correlate with more negative (bluer) β slopes. As β provides insight into dust attenuation (although with some nuances – see **?** and references therein), galaxies with more negative slopes may be expected to have higher EW values, as dust extinction plays a key role in hindering Lyα escape from galaxies (Blanc et al., 2011; Hagen et al., 2014). However, we do not find any statistically significant relationship between β slope and Lyα EW (ρ = -0.134, p-value = 0.419).

Next we explore how UV luminosity may relate to Lyα EW values. Other studies at $2 < z < 7$ typically find that fainter galaxies tend to have larger EW(Lyα) (Stark et al., 2010; Jones et al., 2012; Oyarzún et al., 2017; Du et al., 2018; Santos et al., 2020; Jones et al., 2023a). This may be expected, as brighter galaxies typically have evolved to larger stellar masses, which is correlated with higher dust content, leading to the destruction of Lyα photons, and an older stellar population (e.g. Silva et al., 1998). Similarly, other studies have found an increase in the escape fraction of Lyα in galaxies with lower UV luminosities (Prieto-Lyon et al., 2022; Saldana-Lopez et al., 2023; Mascia et al., 2023b).

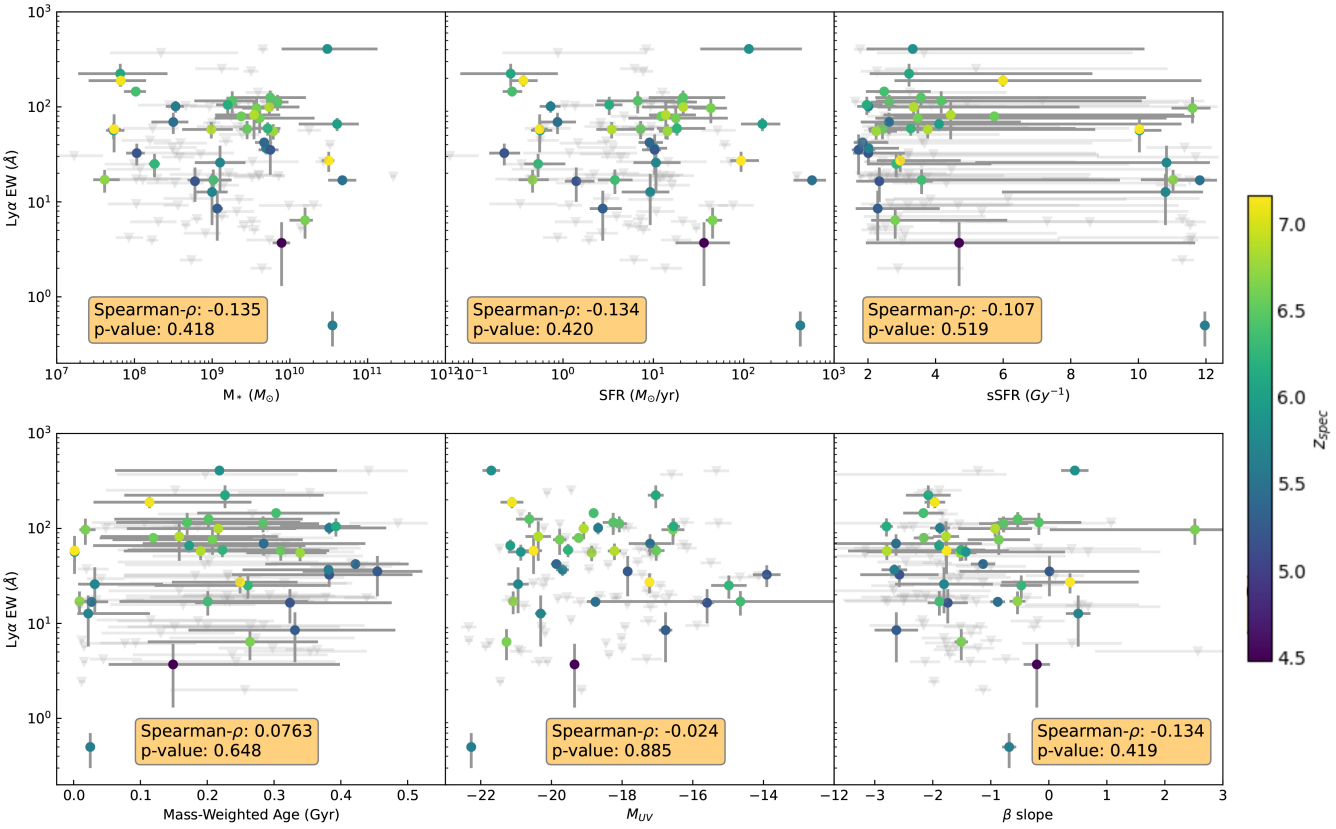

Figure 3.2: Lyα EW vs various stellar and UV properties: stellar mass (M^*), SFR, sSFR, mass-weighted age, $M_{\rm UV}$, and UV β slope. The Spearman correlation coefficient (ρ) and p-value are shown as insets for each corresponding property. We show upper limits from nonemitters which have at least 50% of their $P(z)$ within the Lyα detection range as faint, inverted grey triangles. While there is some evidence of anticorrelation between Lyα EW and physical parameters, none of them are statistically significant.

These may suggest that UV fainter galaxies have stronger Lyα emission. However, our results show no significant relationship between the two properties for our sample (ρ = -0.024, p-value = 0.885 − see Figure 3.2). We also compare the delensed Lyα line luminosity to the intrinsic UV luminosity and find strong and significant anticorrelation ($\rho = -0.591$, p-value=$9.22e^{-5}$)., i.e. more intrinsically UV luminous galaxies exhibit Lyα emission that is significantly stronger than their UV fainter counterparts. Such a trend is expected in our data given the lack of a significant relationship between EW(Lyα)-$M_{\rm UV}$ among LAEs presented in this study.

3.4.2 Stellar Properties

The properties considered in this section concern stellar populations and are determined from SED fitting. We find no evidence of any significant relationships between these SED-fit properties and EW(LYα) in our sample, as can be seen in Figure 3.2. Along the same line of reasoning as why UV fainter galaxies may have stronger Lyα EW, previous studies have found stronger EW values in relatively lower mass galaxies between $2 < z < 6$. Pentericci et al. (2007); Blanc et al. (2011); Nilsson et al. (2011); Hagen et al. (2014); Oyarzún et al. (2016, 2017); Du et al. (2018); Pucha et al. (2022) all report an anticorrelation between EW and stellar mass to varying degrees of significance. However, Kornei et al. (2010) and Hathi et al. (2016) do not find any significant correlation between the two quantities in their samples, although Kornei et al. (2010) observations are missing near-IR photomettry to accurately determine masses.

The relationships found in literature between star formation rates and Lyα EW generally points toward less star-forming galaxies having larger EW values. (e.g. Kornei et al., 2010; Hathi et al., 2016; Oyarzún et al., 2017; Trainor et al., 2019; Ortiz et al., 2023). However, Marchi et al. (2019) and Pucha et al. (2022) do not find any correlation between EW and SFR in galaxies between $2.5 < z < 4.5$. Our results align with the latter cases, as we find no significant evidence that the two parameters are related. We also estimate specific star formation rates and how Lyα EW depends on it, and do not find any statistically significant relationship between sSFR and Lyα emission strength (see Figure 3.2 upper middle and right panels).

The relationship between age and Lyα EW has perhaps the most varied results in the literature. We find no relationship between mass-weighted age and Lyα EW in our sample, but also note the large errors on some age values, which can be seen in Figure 3.2. Some studies spanning $2 < z < 6$ have found that higher EWs are found in older galaxies (Kornei et al., 2010; Marchi et al., 2019; McCarron et al., 2022), some have found the opposite trend (Pentericci et al., 2007; Santos et al., 2020; Reddy et al., 2022), and others find no correlation (Pentericci et al., 2009). Ages are also highly dependent on the SFH chosen during SED fitting. As mentioned earlier, we also estimate the ages for this sample using a delayed-τ SFH. While the ages are consistently lower for a delayed-τ SFH relative to those derived

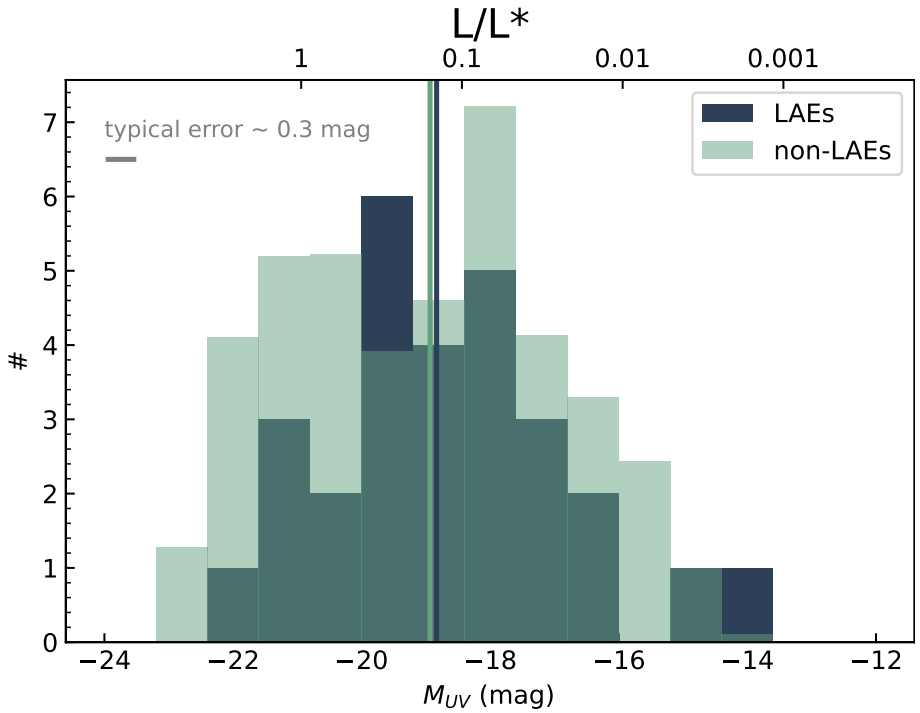

Figure 3.3: Distribution of intrinsic UV luminosity for LAEs vs nonemitters, calculated on the peak of the photometric redshift distribution for nonemitters if it falls within the Lyα detection range, and the center of the range if not. Values for the nonemitter population are weighted by the product of the fraction of $P(z)$ within the range where Lyα could be detected and the fraction of EW calculation MC iterations for which the 3σ EW limit is $\leq$ 25Å.

using a constant SFH, there still remains no significant relationship between Lyα EW and mass-weighted age. We discuss possible physical and statistical reasons behind the lack of significant correlations in our sample in depth in Section 3.7. For all the properties, in addition to the p-values showing insignificant relationships, the absolute value of ρ is small in all cases, such that even if there was a significant correlation or anticorrelation, it would be weak.

3.5 Comparing LAEs and Nonemitters

In order to gain insight into what may be driving the escape of Lyα photons in LAEs, we also compare the distributions of the six physical properties explored above for both LAEs and nonLAEs, using the cutoff of Lyα EW $\geq$25Å to define the LAE sample. Galaxies which have detected Lyα emission measured at ¡ 25Å EW are also placed into the nonemitter sample. While there are slight deviations in the distributions, we do not find any significant differences between any of the six properties of LAEs and nonemitters based on the results

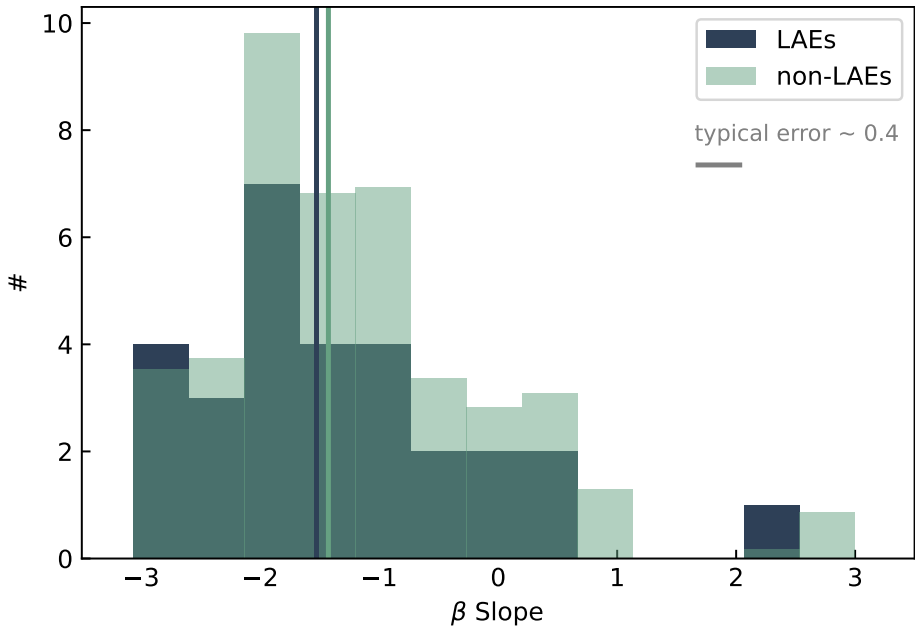

Figure 3.4: Distribution of UV β slope for LAEs vs nonemitters. We note that the LAE with a slope ¿ 2 only had photometric data from two filters (F140W and F160W) and both detections were at the edge of the observational limit ($m_{\rm AB} \sim 29$ with large errors). Positive values for nonLAEs either have a similar situation with only two photometric fluxes or could be the effect of low-z interlopers which are downweighted but still enter the distribution. Values for nonLAEs are weighted using the process described in Section 3.3.4.

of both two-sample Kolmogorov-Smirnov (KS) tests and Mann-Whitney U tests. Previous studies have found statistically significant differences between the populations of LAEs and nonemitters (e.g. Pentericci et al., 2007; Stark et al., 2010; Jones et al., 2012; Napolitano et al., 2023). However, others such as Hathi et al. (2016) generally do not. Very broadly, LAEs have been found in past works to be generally lower mass, fainter, and have less dust and bluer β slopes than nonLAEs, but there are some inconsistent results across different surveys. Potential explanations for our lack of significant differences are discussed further in Section 3.7.

We compare the $M_{\rm UV}$ distributions of emitters and nonemitters. As discussed earlier, candidates without spectroscopic confirmation have some uncertainty in their $M_{\rm UV}$, dominated by the uncertainty in z and consequently d_L. To mitigate this when comparing the luminosities of LAEs and non-emitters, we perform a similar MC sampling as described in Section 3.3.4. In KS tests comparing the $M_{\rm UV}$ distributions of LAEs and nonemitters in this iterative process, a typical p-value is between 0.2 and 0.4, with none below 0.005, and thus,

we do not have sufficient evidence to reject the null hypothesis that the two samples are drawn from the same .

In Figure 3.3, we show the distribution of $M_{\rm UV}$ values for the LAEs against those of the nonemitters, calculated from the peak $z_{\rm phot}$ value if it is within the desired redshift range, or the middle value of the range if it is not. Each data point in the latter distribution is weighted by the product of fraction of total $P(z)$ within the desired redshift range and the fraction of Lyα EW determinations which are below 25Å, as described in section 3.3.4. The $M_{\rm UV}$ distribution of LAEs covers a broader range of luminosities, and also has a slightly lower median, although the tests reveal no statistical difference. Lemaux et al. (2021) use the $5 < z < 7$ galaxies as part of a larger sample and compare the LAE fraction for the bright ($L \sim 0.67L^*$) and faint ($L \sim 0.1L^*$) counterparts in and find a higher fraction of LAEs in the faint bin. This may be explained by there being a higher percentage of LAEs among faint galaxies.

We also find there to be no significant difference between the β slopes of LAEs and nonemitters, although the median β of LAEs is slightly more negative than that of nonemitters. Both simulations (Verhamme et al., 2008) and studies at lower redshifts (Hayes et al., 2011; Atek et al., 2014) suggest that dust inside of galaxies prevents Lyα photon escape. We therefore initially expect that LAEs may tend to have bluer UV slopes, indicating lower dust content. While we find that the median β slope value for LAEs is slightly bluer than that of nonemitters, a KS test indicates no significant difference between the two populations. Figure 3.4 shows the distribution of β slopes for the LAE sample and the nonemitter sample, with the same weighting scheme as used in Figure 3.3.

For the SED-derived properties of stellar mass, SFR, sSFR, and age, a KS test indicates no statistically significant difference between any of these properties for LAEs vs nonemitters. The distributions can be seen in Figure 3.5, where the nonLAE properties are weighted using the same prescription as described previously. Between the samples, when employing both a KS and Mann-Whitney test, we do not find any significant difference. The resultant p-values all indicate there is not much evidence that the two samples come from different parent distributions.

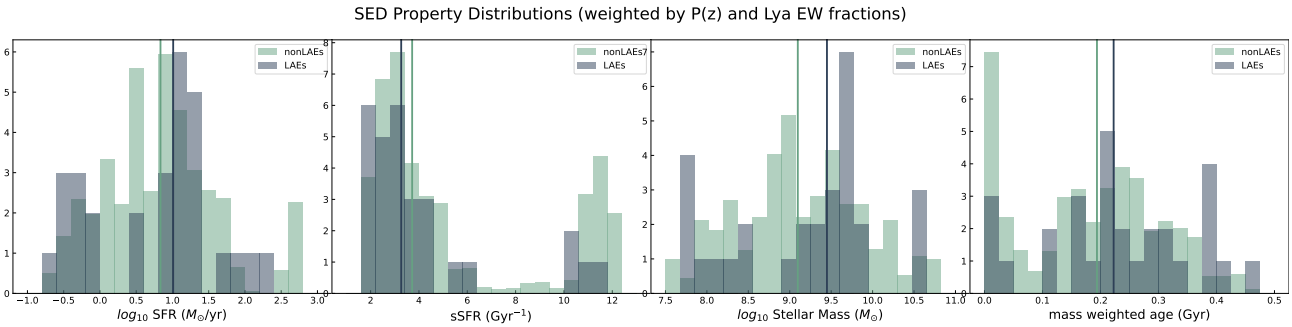

Figure 3.5: Distribution of estimated stellar properties from SED fitting for LAEs vs nonemitters. Solid vertical lines indicate the median value of the distribution with the corresponding color.

3.6 Spectral Properties of LAEs at $z \sim 7$

Lyα is typically the brightest UV line in EoR galaxies, making it the first emission line that is typically targeted in an attempt to confirm a redshift of such galaxies. However, it is not present in every galaxy and also has a tendency to be scattered by neutral hydrogen, leading to a redshift value that is offset from systemic. For this reason, detecting an alternate, non-resonant emission line can help to gain insights into the ISM state of galaxies as well as determine the true redshift (e.g. Dijkstra, 2014; Yang et al., 2017; Guaita et al., 2017; Mason et al., 2018; Cassata et al., 2020). We selected six spectroscopically confirmed LAEs at $z \sim 7$ to follow up with Keck/MOSFIRE to look for CIII] 1907, 1909 Å emission, whose properties are listed in Table 3.2. Five of the six are included in all previous analyses, and the sixth, coined DP7, has a strong Lyα detection described by Pelliccia et al. (2021). DP7 is not included in our sample as it was targeted separately in a different survey program, the Reionization Lensing Cluster Survey (RELICS; Coe et al., 2019). For all previous analyses, we treat the triply imaged LAE detected in the field of the cluster MACS2129 as one target and do all SED fits on the photometry of the brightest image, Image A. Three full nights were awarded to the project, and we observed for an additional two half nights for a total of 35 hours on sky.

The reduction of the data was done using the pipeline developed by the MOSFIRE Deep Evolution Field (MOSDEF) survey (Kriek et al., 2015). This process accounts for any potential instrumental drift as well as any differential atmospheric diffraction by tracking a star in one of the slits, ensuring that minimal signal is lost when combining frames, which is especially pertinent for faint galaxies. After recovering no obvious emission lines

$z \sim 7$ LAE Properties

Galaxy Name	α_{J2000} (deg)	δ_{J2000} (deg)	$z_{\mathrm{Ly}\alpha}$	$\mathrm{EW}_{\mathrm{Ly}\alpha}$ (Å)	Ref[a]	t_{obs} in H band (min)	$\mathrm{EW}_{\mathrm{CIII]}}$ (Å, 3σ)
MACS0744-064	116.24648	39.46042	7.148 ± 0.001	58.3 ± 25.1	[1]	360	¡ 43.95
MACS1423.16	215.928929	24.072848	7.101 ± 0.001	189 ± 25	[2]	490	¡ 28.08
MACS2129-A	322.350936	7.693322	6.846 ± 0.001	60 ± 11	[3]	318	¡ 20.20 (stacked)
MACS2129-B	322.353239	7.697442	6.846 ± 0.001	47 ± 9	[3]	318	...
MACS2129-C	322.353943	7.681646	6.846 ± 0.001	170 ± 77	[3]	318	...
RXJ1347-018	206.89124	11.75261	7.161 ± 0.001	27.2 ± 6.5	[1]	354	¡ 27.38
RXJ1347.47	206.900859	-11.754209	6.771 ± 0.001	55.4 ± 10.2	[2]	354	¡ 22.91
DP7	152.6593385	12.6556351	7.0281 ± 0.0003	237.12 ± 57.78	[4]	672	¡ 47.18

[a] References for Lyα detections: [1]Hoag et al. (2019), [2]Fuller et al. (2020), [3] Huang et al. (2016b), [4]Pelliccia et al. (2021).

Table 3.2: LAE Properties of $z \sim 7$ galaxies used in spectroscopic CIII] emission search

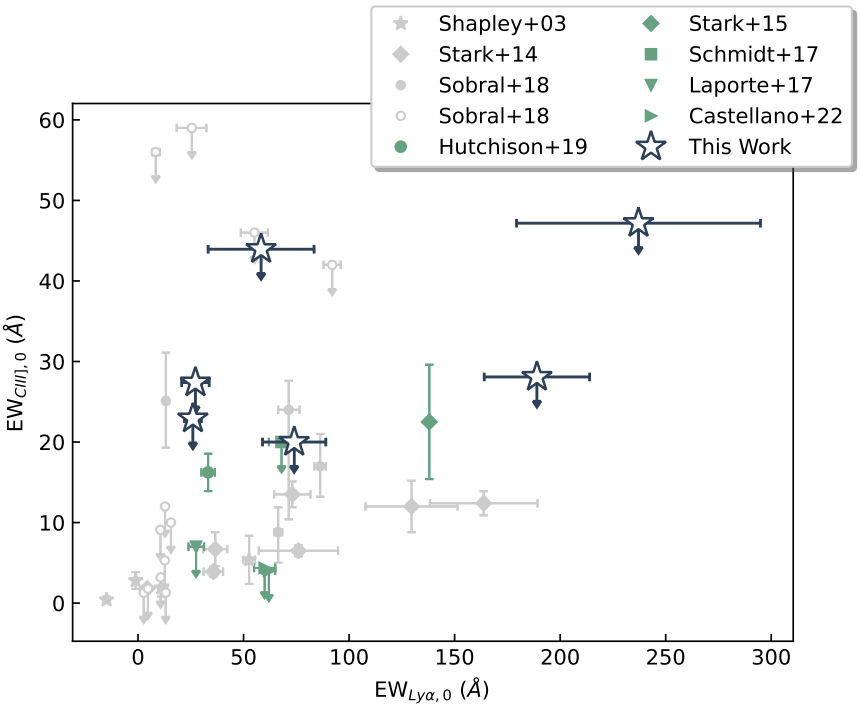

Figure 3.6: Lyα vs CIII] EW value or upper limits for LAEs

in a by-eye search from the initial reductions, we stress test the frames to guarantee that no signal was missed. These tests include varying the width of the boxcar used in the 1D extraction, removing frames where there was cirrus cloud coverage, and performing an automated integrated signal to noise ratio search in addition to probing the reduced spectra by eye. After testing each reduced galaxy meticulously, we confirm that there is no CIII] emission detected from any of the targeted galaxies.

We also perform a test for faint CIII] emission by stacking the spectra of all six LAEs to see if there is any significant signal to noise recovered. In this process, we use the Lyα Δv distribution from Cassata et al. (2020) as CIII] should trace the systemic velocity of the galaxy (e.g. **??**). We sample an offset from this distribution for each of the six LAEs, shift the spectrum by that amount, and perform an inverse variance weighted stacking at that location. Over all iterations, we recover no appreciable integrated signal-to-noise at the expected location of CIII]. Figure 3.7 shows the distribution of the stacked integrated signal-to-noise ratio (SNR) across the spectral window where CIII] would be expected for 1000 iterations.

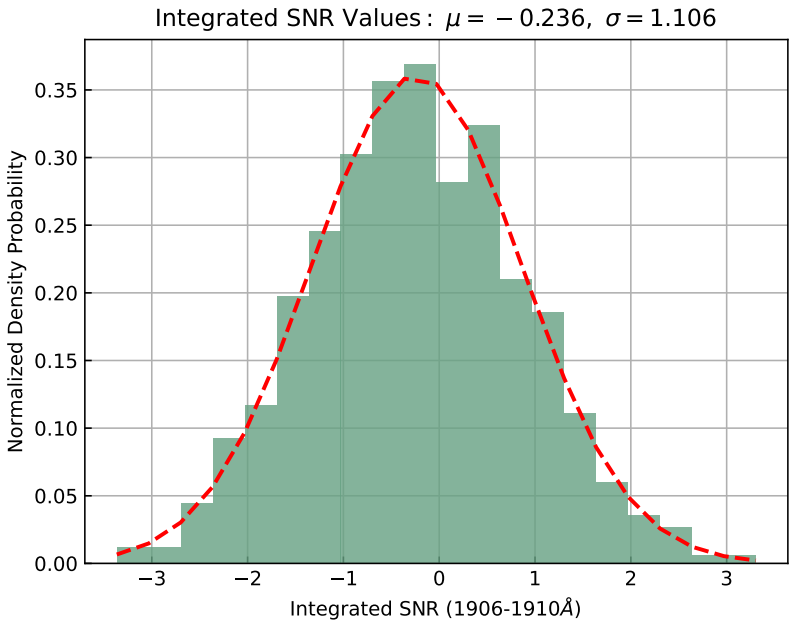

Figure 3.7: Distribution of integrated stacked SNR values for the six galaxies used in the CIII] search. These values give no indication of any CIII] emission when stacking the spectra of all the galaxies. The red dashed line shows a Gaussian fitted to the distribution. The slightly negative peak value may indicate modest background oversubtraction during reduction.

Even with no detected CIII], we can use the upper limits on the relative strength of the individual lines as well as the stacked limit to gain insights into these LAEs and rule out certain characteristics. For each galaxy targeted, we compute the 1σ upper limit on the rest-frame EW of CIII] using the same process as described in section 3.3.3. The 3σ upper limits on the EW of CIII] are noted in Table 3.2 and plotted in Figure 3.6. We calculate a stacked EW limit on CIII] of 8.6Å at the 3σ level for all of the galaxies together.

Typical CIII] EW values from the $z \sim 2-3$ universe are less than 15Å with a median value around 7Å (Stark et al., 2014; Llerena et al., 2022). Sources at higher redshifts however have detected CIII] emission at higher EW values. Stark et al. (2015), Hutchison et al. (2019), and Topping et al. (2021) classify CIII] emission lines at $z = 6.027, z = 7.51$, and $z = 7.945$, and with EW values for the combined doublet of 22.5± 7.1Å, 16.23± 2.32Å, and 20.3± 6.5Å, respectively. Recent NIRSpec observations by Tang et al. (2023) find CIII] emission in three galaxies at $7.8 < z < 8.7$ with EW values ranging from 10.9-16Å. At high redshifts, there is evidence of stronger CIII] emission than in lower-z galaxies. In addition, observations

from the lower redshift universe have shown a correlation between Lyα EW and CIII] EW (Llerena et al., 2022). Considering these, we may expect some high EW CIII] emitters in our $z \sim 7$ subsample, but we do not and constrain the 3σ stacked EW limit to 8.6Å, a lower value than any of the high-z detected CIII] lines cited above.

Photoionization modelling of confirmed strong CIII] emitters reveals certain properties that allow for the increased production of doubly ionized carbon (e.g. Hutchison et al., 2019). Observations of strong CIII] in lower redshift galaxies have found that such measurements are found in galaxies with low metallicity, high ionization parameters, and hard ionizing spectra (Erb et al., 2010; Steidel et al., 2016; Du et al., 2020; Tang et al., 2021). Hutchison et al. (2019) use their detection as well as limits on other nebular emission lines to determine that the galaxy in study has subsolar metallicity, a high ionization parameter, and a young stellar population. Comparing to models presented in Nakajima et al. (2018a,b), we cannot rule out AGN activity, but galaxies with low CIII] EW limits, like some of those in our subsample, are more likely to be star-forming galaxies than have AGN activity, and also less likely to have extremely high ionization parameters. This is perhaps surprising given that some of the targeted sample has very strong observed Lyα and the similarity of the strength of the Lyα emission relative to other EoR galaxies that have strong observed CIII] emission.

3.7 Discussion

Perhaps the most interesting results from this study are those presented in Sections 3.4 and 3.5: the lack of any significant correlations or differences where they may be expected from previous studies. We find no significant differences between any of the distributions of properties of LAEs and LBG candidates without Lyα emission, as well as no significant correlation between Lyα EW and physical properties for those with spectroscopic detections. Out of the numerous studies which look at the physical differences between LAEs and nonemitters in order to pinpoint what about the emitters allows for the escape of moderate to strong Lyα emission, many studies generally find a consensus that LAEs are bluer, less massive, less star-forming, and fainter. There is scatter within these results, however. Below we discuss both physical and statistical reasons which may explain our results.

Our conclusions may be different than those of other surveys likely due to two properties

of our sample which set it apart from others: high redshifts and faint UV luminosities. Most other studies which perform similar analyses at faint luminosities are at redshifts of $z < 6$. Galaxies in the early universe are more difficult to study and characterize and may be fundamentally different than those at similar stages of evolution at lower redshifts, largely due to their light being at least partially obscured by the opacity of the IGM.

The environment in which these galaxies are formed and existing is a key facet to consider. The IGM is at least partially neutral at $z \gtrsim 6$, with lingering patches of neutral hydrogen possibly present at lower redshifts (e.g. Stark et al., 2010; Mason et al., 2018; Bolan et al., 2022), potentially affecting each galaxy in this study. As neutral hydrogen absorbs the resonant Lyα line, the EW values we obtain may be artificially lower than what has intrinsically escaped the galaxy. Due to the patchiness of reionization (Furlanetto et al., 2006; Treu et al., 2013; Sobacchi & Mesinger, 2014), this effect may not be homogeneous across all galaxies in differing fields of view. A similar consideration is the evidence of overdensities of galaxies at the same redshift within a small physical region, which have been found at $z > 6$ (Castellano et al., 2018; Larson et al., 2022; Jung et al., 2022; Morishita et al., 2023; Hashimoto et al., 2023; Cooper et al., 2023). Perhaps galaxies which reside within these overdense regions have more of a chance of their Lyα photons escaping into the IGM due to the expanse of the ionized bubbles in which they reside. As our study probes 10 lines of sight, this effect is mitigated, but could still have some impacts. The side effects of an evolving IGM and patchy overdensities may cause our EW values to be affected sporadically, leading to the lack of strong correlations between Lyα EW and physical properties. In this case the relationships between physical quantities and Lyα EW could be changed or even completely erased by modulation from the environment. However, we note that Jones et al. (2023a) and Napolitano et al. (2023) both study galaxy samples that extend into the EoR up to $z \sim 8$ and do find anticorrelation with Lyα EW and UV luminosity and dust extinction, respectively, but they study more luminous samples.

We test if modulation by an opaque IGM is a significant factor by looking at how the Lyα EW trends for emitters change when only including galaxies at $z \leq 6$, when the Universe was likely mostly ionized (e.g. Fan et al., 2006a). We find that the significance of the expected anticorrelation between EW and stellar mass and SFR increases, to the $\sim 1.5\sigma$ level. While

this is still not strong enough to confidently claim a correlation, it is perhaps indicative that the increasingly neutral IGM at redshifts above $z \sim 6$ may play a role in our results.

In addition to the environment in which the galaxies are forming, this sample is unique in that it is comprised of LBG candidates which are characteristically faint ($< L^*$), observable due to magnification from massive lensing clusters. The $M_{\rm UV}$ distribution of our sample is much fainter than that of any other surveys to which we compare; the typical value of the intrinsic absolute UV magnitude of the galaxies in our sample is ~ -19, reaching down to $M_{\rm UV} \sim -14$, whereas other comparison surveys generally probe galaxies closer to L^*, at absolute magnitudes of $-22 \lesssim M_{\rm UV} \lesssim -18$. We are exploring unchartered phase spaces in this study, as there have been no surveys at these redshifts with galaxies as faint as those in our sample. The most similar sample is the recent one from JADES with spectroscopy from *JWST* NIRspec presented by Jones et al. (2023a), who do find the expected correlation between Lyα EW and $M_{\rm UV}$, but do not have low-luminosity galaxies with EW values in the 10-100Å range, where our sample does include some of these. As noted in McCarron et al. (2022), low-mass, low-EW systems are notoriously hard to study, so often samples are comprised of more rare bright LAEs, which may not be representative of the typical galaxy population. While our survey is certainly not insusceptible to Malmquist bias, gravitational lensing does allow for some mitigation of its effects. We detect these types of galaxies that are missed in field surveys, but whose physical properties veer away from the tight correlations that are presented in other works, as can be seen in the bottom center panel of Figure 3.2.

Our lack of correlations among Lyα line strength of LAEs and their physical properties may be not only due to the faint galaxies we detect with low Lyα EW, but also the large scatter we see at the high luminosity end of our sample. We see both our highest and lowest Lyα EW at bright luminosities. Our sample is characteritstically faint, and we do not have a large number of galaxies brighter than $M_{\rm UV} \sim -21$. Many other samples cover brighter UV luminosities; perhaps if brighter targets were probed, we would recover the low EW values seen in other surveys and see correlations or more difference between the LAE and nonemitter populations. These results may suggest that the fainter population of galaxies are inherently different from their bright counterparts as they do not exhibit the same significant trends.

Lastly, we also consider our sample size. While we have spectroscopic data on 247 galaxies and LBG candidates, we have 38 which are confirmed to be at $5 < z < 8.2$ from Lyα emission, and the rest have photometric redshifts with varying degrees of certainty to be within the range where we could detect Lyα emission. When we weight each nomemitter using the scheme defined in section 3.3.4, the size of the effective nonemitter sample is comparable to that of the emitters. Perhaps the intrinsic scatter shrouds any correlations or population differences with a relatively small sample size. We note that the uncertainty in redshift for the nonemitters may affect these results; however, those LBG candidates which are most likely to be at the redshifts we are studying are the ones which make the most contribution to the comparison between LAEs and nonLAEs.

We perform tests to see if significant correlations that are evident in a large sample would be detectable with our sample size. First, we take the data from the VIMOS Ultra Deep Survey (VUDS; Le Fèvre et al., 2015; Tasca et al., 2017; Lemaux et al., 2022), a spectroscopic survey of galaxies with $0.3 < L_{\rm UV}/L^* < 3$ over the redshift range $2 < z < 6$, which has spectroscopic observations that are integrated for long enough to reach the continuum, such that Lyα in emission is not requirement for a redshift. These which show weak ($\rho = -0.18$) anticorrelation between Lyα EW in emission and SFR at $> 5\sigma$ significance at $2 < z < 6$. From this data, we subsample a random draw of 38 galaxies and compute the Spearman correlation statistic and p-value between Lyα EW and SFR. Over all iterations of this subsampling, only $\sim 3\%$ show a $> 3\sigma$ significance. We note that we are not directly comparing the results of this survey with ours as they are at different redshift ranges, but simply using the sample to see if weak correlations found in large samples would be evident in one of our size. These results show that we may not recover a similarly weak trend with our sample size.

We apply the same method to the data presented by JADES (Jones et al., 2023a), whose original sample shows strong correlation ($\rho = 0.65$) between Lyα EW and $M_{\rm UV}$ at $> 5\sigma$ significance at a similar redshift range to ours, $3 < z < 8$. When we perform the subsampling, all iterations result in strong correlations. All realizations return significances of $> 2\sigma$, and the vast majority show a $> 3\sigma$ significance. These exercises show that if a strong correlation exists in the underlying population of galaxies, a sample of our size would

likely show that correlation. However, as we do not find any evidence of correlation between Lyα EW and any of the physical properties studied, we conclude that, if there does exist a trend among the underlying population of galaxies we probe, it is weak at best.

Our lack of expected correlations or differences between LAEs and nonemitters among sub-L^* galaxies is likely due to some combination of environmental effects, specifically inhomogeneous IGM opacity, and a fainter sample than is typically studied. It is unlikely to be solely due to having a low sample size − if a strong correlation exists among an underlying population, it would still likely show at high significance in a small subsample. Our inclusion of low Lyα EW, low luminosity galaxies as well as bright, large EW galaxies may reduce correlation strength in the properties we study, and also contribute to the similar distributions among LAEs and nonLAEs. The correlations between Lyα EW and physical properties such as stellar mass, SFR, UV luminosity, and β slope, appear to be weaker among faint $z > 5$ galaxies than some other samples suggest.

3.8 Conclusions

We have analyzed the stellar and UV properties of a sample of 247 faint, gravitationally lensed LAEs and LBG candidates between $5 < z < 8.2$ with both deep photometric and spectroscopic data. We investigate how Lyα EW correlates with UV and stellar properties for galaxies with detected emission, and we also compare the distributions of these properties for LAEs and the nonLAE sample.

- We do not find any significant correlations between Lyα EW and any of the stellar or UV properties which we analyze in this work.
- We find no significant difference between the stellar and UV properties of LAEs and nonemitters.
- Our lack of correlations indicate that if trends exist in this population of faint EoR galaxies, they are weak. We detect low-EW, faint galaxies which other surveys do not, and also have high scatter in properties at the bright end of our sample. Our results could also be modulated by suppressed Lyα emission due to a partially neutral IGM at these redshifts. Any weak trends could be rendered less significant by the uncorrelated

opacity of the surrounding IGM.

- We do not find CIII] emission in a spectroscopic search of six confirmed LAEs at $z \sim 7$ and calculate their EW upper limits, some of which are constraining enough to rule out extreme nebular emission properties and disfavor AGN as being the dominant source powering emission.

  Continued observations of high-z galaxies with $JWST$ will allow for large sample sizes of EoR galaxies with confirmed redshifts and the necessary data to confidently estimate physical properties via SED fitting, as well as accurate β slopes from spectra. Even in the era of $JWST$, large samples of ground-based observations are important for detecting low EW Lyα lines at these redshifts, as it is difficult even with the NIRSpec prism. Taking advantage of these and future observations in the coming years will narrow down the properties which drive Lyα and ionizing photon production and escape in EoR galaxies, allowing for the characterization of the sources which caused cosmic reionization.

Acknowledgements

We acknowledge support from the program HST-GO-16667, provided through a grant from the STScI under NASA contract NAS5-26555. MB acknowledges support from the ERC Grant FIRSTLIGHT and Slovenian national research agency ARRS through grants N1-0238 and P1-0188. Based on spectrographic data obtained at the W.M.Keck Observatory, which is operated as a scientific partnership among the California Institute of Technology, the University of California, and the National Aeronautics and Space Administration. The Observatory was made possible by the generous financial support of the W.M. Keck Foundation. The authors wish to recognize and acknowledge the very significant cultural role and reverence that the summit of Maunakea has always had within the indigenous Hawaiian community. We are most fortunate to have the opportunity to conduct observations from this mountain. Also based on observations made with the NASA/ESA Hubble Space Telescope, obtained at the Space Telescope Science Institute, which is operated by the Association of Universities for Research in Astronomy, Inc., under NASA contract NAS5-26555. And based on observations made with the Spitzer Space Telescope, which is operated by the

Jet Propulsion Laboratory, California Institute of Technology under a contract with NASA. Support for this work was also provided by NASA/HST grant HST-GO-14096, and through an award issued by JPL/Caltech. PB thanks Spencer Fuller, Austin Hoag, and Charlotte Mason for their immense contributions to this work, having designed and executed many of the observations, data reduction, and preliminary analyses. We also thank Gareth Jones for access to the data presented in his work which we use for comparisons in this analysis.

Chapter 4

Summary and Conclusions

In this dissertation, I have discussed my contributions to the field of high-redshift astrophysics and the Epoch of Reionization. I use a large sample of characteristically faint, gravitationally lensed EoR galaxies with a range of physical properties to address open questions concerning the first billion years of the Universe's existence. As faint galaxies are likely to have emitted large amounts of ionizing photons which fueled cosmic reionization, they are the perfect subjects with which to study this epoch. I present the various ways that this sample is used to explore reionization.

Having a large sample of characteristic galaxies gives access to a perspective on the early universe that is unattainable with bright galaxies alone. In Chapter 2, I discuss a study on the timeline of reionization, using this sample to infer the neutral fraction of hydrogen at various redshifts in the EoR. Using the relative changes in Lyα emission strength and frequency across different redshift bins among physically similar galaxies allows for tight constraints on the estimated neutrality of the IGM. In Chapter 3, I show how these galaxies are used to profile typical emitters of the bulk of ionizing photons. I measure and estimate various physical properties of the entire sample and compare the distributions of LAEs and nonLAEs. I also look at how these properties relate to Lyα equivalent width for those with detected emission. In this chapter, I also discuss how a lack of strong CIII] emission in $z \sim 7$ galaxies can rule out certain extreme physical conditions.

4.1 Future of the Field

Astronomy is entering into an exciting era of massive space and ground based observatories which are and will continue to accelerate humanity's knowledge of the cosmos. Due to the successful deployment of the *JWST* at the end of 2021, the past year have seen a massive uptick in high-redshift galaxy observations and research. In particular, early surveys such as CEERS (Finkelstein et al., 2023), GLASS (Treu et al., 2022), and CANUCS (Willott et al., 2022), JADES (Bunker et al., 2023), and COSMOS-Web (Casey et al., 2023) have made impressive leaps in the sample sizes of photometrically selected and spectroscopically detected high-z galaxies, with some galaxies being spectroscopically confirmed at $z > 10$ (Bunker et al., 2023; Curtis-Lake et al., 2023).

These early surveys have been used to constrain the properties of EoR galaxies and the state of the IGM at various redshifts, expanding upon the work done in this dissertation. Through detection of rest-frame optical emission and absorption features, the ISM properties of early galaxies are being studied in detail. With access to these emission lines, direct gas-phase metallicities and relative chemical abundances have been measured at an unprecedented level in galaxies at $z > 6$. Generally, studies which explore these parameters have found high ionization parameters and subsolar metallicities (e.g., Arellano-Córdova et al., 2022; Curti et al., 2022; Bunker et al., 2023; Trump et al., 2023; Saxena et al., 2023b; Mascia et al., 2023b; Tang et al., 2023; Tacchella et al., 2023; Cameron et al., 2023; Shapley et al., 2023; Sanders et al., 2023; Nakajima et al., 2023; Simmonds et al., 2023). In addition, galaxies whose luminosities exceed expectations at their redshift values have been discovered (e.g., Tang et al., 2023; Donnan et al., 2022; Harikane et al., 2023). Similarly, high-z AGN are being found in *JWST* spectra, perhaps at higher redshifts and in higher numbers than would be expected with current cosmological models (e.g., Juodžbalis et al., 2023; Larson et al., 2023). These results represent a huge step forward in determining a detailed history of how reionization occurred. Insights on the physical properties and ionizing mechanisms of the first light emitters are the first step in revealing exactly how the IGM transitioned to ionized hydrogen and the sources which were primarily responsible.

In addition to future space-based observatories, there are many planned for here on the ground. Some should see first light within a decade with primary mirrors in excess of 20

meters, including the Giant Magellan Telescope, Thirty Meter Telescope, and the Extremely Large Telescope. The large field of view and sensitivity of the Giant Magellan Telescope will aid in high-z discoveries (GMT Science Advisory Committee, 2018), and the Thirty Meter Telescope will provide observations of faint EoR galaxies, pushing to lower luminosities than possible with *JWST* (Trancho, 2022). The European Extremely Large Telescope aims to shed light on the formation and evolution of the first stars and galaxies in the EoR and their role in cosmic reionization by using high spatial resolution imaging and spectroscopy of these light sources (E-ELT, 2009). The Atacama Large Millimeter/submillimeter Array (ALMA) has been instrumental in detecting the rest-frame infrared emission on early galaxies and will continue to be useful in constraining their dust contents. With the threat of extreme light pollution in the night sky from increasingly more satellites, ground based astronomy as we know it may be evolving. But there will still be countless ways to discover the cosmos, and the field will adapt to overcome the challenge.

This is a very exciting time for the field of astronomy. From the search for habitable exoplanets, to images of black holes, to detection of the first galaxies to form in the Universe, we are making discoveries that could not have been predicted. The upcoming large-aperture observatories that will emerge on the scene in the following decade are sure to continue the outpouring of scientific advances that have been found in recent years. The data from current and new observatories in the coming decades may finally answer the primary questions addressed in this dissertation. The Epoch of Reionization may no longer be shrouded in mystery, with the future of astronomical studies furthering mankind's exploration of space, time, and self.

References

Achúcarro, A. et al. 2022, Inflation: Theory and Observations, arXiv:2203.08128 [astro-ph, physics:hep-ph, physics:hep-th]

Adams, N. J. et al. 2022, Monthly Notices of the Royal Astronomical Society, 518, 4755

Arellano-Córdova, K. Z. et al. 2022, ApJL, 940, L23

Atek, H., Kunth, D., Schaerer, D., Miguel Mas-Hesse, J., Hayes, M., Östlin, G., & Kneib, J.-P. 2014, A&A, 561, A89

Barnacka, A. 2018, Physics Reports, 778-779, 1

Bañados, E. et al. 2018, Nature, 553, 473

Becker, G. D., Davies, F. B., Furlanetto, S. R., Malkan, M. A., Boera, E., & Douglass, C. 2018, The Astrophysical Journal, 863, 92

Becker, R. H. et al. 2001, The Astronomical Journal, 122, 2850, arXiv:astro-ph/0108097

Begley, R. et al. 2022, Monthly Notices of the Royal Astronomical Society, 513, 3510

Bertin, E., & Arnouts, S. 1996, Astron. Astrophys. Suppl. Ser., 117, 393

Blanc, G. A. et al. 2011, ApJ, 736, 31

Bolan, P. et al. 2022, Monthly Notices of the Royal Astronomical Society, 517, 3263

Bosman, S. E. I. et al. 2021, arXiv:2108.03699 [astro-ph]

Bouwens, R. J., Illingworth, G. D., Oesch, P. A., Caruana, J., Holwerda, B., Smit, R., & Wilkins, S. 2015, The Astrophysical Journal, 811, 140

Bouwens, R. J. et al. 2014, The Astrophysical Journal, 793, 115

——. 2003, The Astrophysical Journal, 595, 589

Bouwens, R. J., Oesch, P. A., Illingworth, G. D., Ellis, R. S., & Stefanon, M. 2017, The Astrophysical Journal, 843, 129

Bradač, M. et al. 2019, Monthly Notices of the Royal Astronomical Society, 489, 99

——. 2014, The Astrophysical Journal, 785, 108

——. 2009, ApJ, 706, 1201

Brammer, G. B., van Dokkum, P. G., & Coppi, P. 2008, The Astrophysical Journal, 686, 1503

Bruzual, G., & Charlot, S. 2003, Monthly Notices RAS, 344, 1000

Buat, V. et al. 2012, Astronomy & Astrophysics, 545, A141

Bunker, A. J. et al. 2023, JADES NIRSpec Spectroscopy of GN-z11: Lyman-{\textbackslashalpha\ emission and possible enhanced nitrogen abundance in a \z=10.60\ luminous galaxy

Cabello, C. et al. 2022, A&A, 659, A116

Cain, C., D'Aloisio, A., Gangolli, N., & Becker, G. D. 2021, ApJL, 917, L37

Calabrò, A. et al. 2021, Astronomy & Astrophysics, 646, A39

Calzetti, D., Armus, L., Bohlin, R. C., Kinney, A. L., Koornneef, J., & Storchi-Bergmann, T. 2000, ApJ, 533, 682

Cameron, A. J. et al. 2023, A&A, 677, A115, arXiv:2302.04298 [astro-ph]

Carnall, A. C. et al. 2022, Monthly Notices of the Royal Astronomical Society: Letters, 518, L45

Carnall, A. C., McLure, R. J., Dunlop, J. S., & Davé, R. 2018, Monthly Notices of the Royal Astronomical Society, 480, 4379

Caruana, J., Bunker, A. J., Wilkins, S. M., Stanway, E. R., Lacy, M., Jarvis, M. J., Lorenzoni, S., & Hickey, S. 2012, Monthly Notices of the Royal Astronomical Society, 427, 3055

Caruana, J., Bunker, A. J., Wilkins, S. M., Stanway, E. R., Lorenzoni, S., Jarvis, M. J., & Ebert, H. 2014, Monthly Notices of the Royal Astronomical Society, 443, 2831

Caruana, J. et al. 2018, Monthly Notices of the Royal Astronomical Society, 473, 30

Casey, C. M. et al. 2023, ApJ, 954, 31

Cassata, P. et al. 2020, A&A, 643, A6

Castellano, M. et al. 2016, A&A, 590, A31

——. 2018, ApJ, 863, L3

Charlot, S., & Fall, S. M. 2000, ApJ, 539, 718

Chisholm, J., Prochaska, J. X., Schaerer, D., Gazagnes, S., & Henry, A. 2020, Monthly Notices of the Royal Astronomical Society, 498, 2554

Chisholm, J. et al. 2022, Monthly Notices of the Royal Astronomical Society, 517, 5104

Cimatti, A., Fraternali, F., & Nipoti, C. 2019, Introduction to Galaxy Formation and Evolution (Cambridge University Press)

Coe, D. et al. 2019, ApJ, 884, 85

Cooper, O. R. et al. 2023, The Web Epoch of Reionization Lyman-{\textbackslashalpha\ Survey (WERLS) I. MOSFIRE Spectroscopy of {\textbackslashmathbf{z \textbackslashsim 7-8}\ Lyman-{\textbackslashalpha\ Emitters

Curti, M. et al. 2022, Monthly Notices of the Royal Astronomical Society, 518, 425

Curtis-Lake, E. et al. 2023, Nat Astron, 7, 622

Davies, F. B. et al. 2018, The Astrophysical Journal, 864, 142

Davé, R. et al. 2001, ApJ, 552, 473, arXiv:astro-ph/0007217

Dayal, P. et al. 2020, Monthly Notices of the Royal Astronomical Society, 495, 3065

De Barros, S. et al. 2017, Astronomy & Astrophysics, 608, A123

Dekel, A., Sarkar, K. C., Birnboim, Y., Mandelker, N., & Li, Z. 2023, Monthly Notices of the Royal Astronomical Society, 523, 3201

Di Criscienzo, M. et al. 2017, A&A, 607, A30

Dijkstra, M. 2014, Publ. Astron. Soc. Aust., 31, e040

Donnan, C. T. et al. 2022, Monthly Notices of the Royal Astronomical Society, 518, 6011

Du, X. et al. 2018, ApJ, 860, 75

Du, X., Shapley, A. E., Tang, M., Stark, D. P., Martin, C. L., Mobasher, B., Topping, M. W., & Chevallard, J. 2020, ApJ, 890, 65

Durkalec, A. et al. 2018, Astronomy & Astrophysics, 612, A42

D'Aloisio, A., McQuinn, M., Maupin, O., Davies, F. B., Trac, H., Fuller, S., & Upton Sanderbeck, P. R. 2019, The Astrophysical Journal, 874, 154

D'Aloisio, A., McQuinn, M., & Trac, H. 2015, The Astrophysical Journal, 813, L38

E-ELT, S. W. G. 2009, An Expanded View of the Universe: Science with the European Extremely Large Telescope

Endsley, R., Stark, D. P., Charlot, S., Chevallard, J., Robertson, B., Bouwens, R. J., & Stefanon, M. 2021, Monthly Notices of the Royal Astronomical Society, 502, 6044, _eprint: https://academic.oup.com/mnras/article-pdf/502/4/6044/36524730/stab432.pdf

Erb, D. K., Pettini, M., Shapley, A. E., Steidel, C. C., Law, D. R., & Reddy, N. A. 2010, ApJ, 719, 1168

Faber, S. M. et al. 2003, Waikoloa, Hawai'i, United States, 1657

Fan, X., Bañados, E., & Simcoe, R. A. 2023, Annu. Rev. Astron. Astrophys., 61, 373

Fan, X., Carilli, C. L., & Keating, B. 2006a, Annual Review of Astronomy and Astrophysics, 44, 415

Fan, X. et al. 2006b, The Astronomical Journal, 132, 117

Fazio, G. G. et al. 2004, ASTROPHYS J SUPPL S, 154, 10

Feroz, F., & Hobson, M. P. 2008, Monthly Notices of the Royal Astronomical Society, 384, 449

Feroz, F., Hobson, M. P., & Bridges, M. 2009, Monthly Notices of the Royal Astronomical Society, 398, 1601

Finkelstein, S. L. et al. 2023, ApJL, 946, L13

——. 2019a, Unveiling the Phase Transition of the Universe During the Reionization Epoch with Lyman-alpha

——. 2019b, The Astrophysical Journal, 879, 36

——. 2015, The Astrophysical Journal, 810, 71

Flury, S. R. et al. 2022, ApJ, 930, 126

Fontana, A. et al. 2010, The Astrophysical Journal, 725, L205

Ford, H., Bartko, F., Bely, P. Y., Broadhurst, T., & Burrows, C. J. 1998, SPIE Proceedings, 3356, 234

Fuller, S. et al. 2020, ApJ, 896, 156

Furlanetto, S. R., Zaldarriaga, M., & Hernquist, L. 2006, Monthly Notices of the Royal Astronomical Society, 365, 1012

GMT Science Advisory Committee. 2018, Giant Magellan Telescope Science Book 2018

Goto, H. et al. 2021, ApJ, 923, 229, arXiv: 2110.14474

Grazian, A. et al. 2016, Astronomy & Astrophysics, 585, A48

Greig, B., Mesinger, A., & Bañados, E. 2019, Monthly Notices of the Royal Astronomical Society, 484, 5094

Guaita, L. et al. 2017, A&A, 606, A19

Gunn, J. E., & Peterson, B. A. 1965, ApJ, 142, 1633

Hagen, A. et al. 2014, ApJ, 786, 59

Haiman, Z., & Spaans, M. 1999, The Astrophysical Journal, 518, 138

Harikane, Y. et al. 2023, ApJS, 265, 5

Harish, S. et al. 2021, arXiv:2111.01173 [astro-ph], arXiv: 2111.01173

Haro, P. A. et al. 2023, Spectroscopic verification of very luminous galaxy candidates in the early universe

Hashimoto, T. et al. 2023, RIOJA I. The core of the highest redshift galaxy overdensity at \z= 7.88\ confirmed by NIRSpec/JWST

Hassan, S., Davé, R., Mitra, S., Finlator, K., Ciardi, B., & Santos, M. G. 2018, Monthly Notices of the Royal Astronomical Society, 473, 227

Hathi, N. P. et al. 2016, A&A, 588, A26

Hayes, M., Schaerer, D., Östlin, G., Mas-Hesse, J. M., Atek, H., & Kunth, D. 2011, The Astrophysical Journal, 730, 8

Hayes, M. J., Runnholm, A., Gronke, M., & Scarlata, C. 2021, ApJ, 908, 36

Hinshaw, G. et al. 2013, The Astrophysical Journal Supplement Series, 208, 19

Hoag, A. et al. 2019, ApJ, 878, 12

Huang, K.-H. et al. 2016a, ApJ, 817, 11

——. 2016b, ApJ, 823, L14

Hunter, J. D. 2007, Computing in Science Engineering, 9, 90

Hunter, L. C., van Zee, L., McQuinn, K. B. W., Garner, R., & Dolphin, A. E. 2022, AJ, 163, 132, arXiv: 2201.07339

Hutchison, T. A. et al. 2019, ApJ, 879, 70

Iani, E. et al. 2023, MIDIS. JWST NIRCam and MIRI unveil the stellar population properties of Ly{\textbackslashalpha\-emitters and Lyman-Break galaxies at z \textasciitilde 3-7

Inoue, A. K. et al. 2018, Publications of the Astronomical Society of Japan, 70

Izotov, Y. I., Guseva, N. G., Fricke, K. J., Henkel, C., Schaerer, D., & Thuan, T. X. 2021, A&A, 646, A138

Izotov, Y. I., Worseck, G., Schaerer, D., Guseva, N. G., Thuan, T. X., Fricke, Verhamme, A., & Orlitová, I. 2018, Monthly Notices of the Royal Astronomical Society, 478, 4851

Jin, X. et al. 2023, ApJ, 942, 59

Johnson, B. D. 2021, The Astrophysical Journal Supplement Series

Jones, G. C. et al. 2023a, JADES: The emergence and evolution of Ly-alpha emission & constraints on the IGM neutral fraction

Jones, T. et al. 2023b, ApJL, 951, L17

Jones, T., Stark, D. P., & Ellis, R. S. 2012, ApJ, 751, 51

Jung, I. et al. 2020, The Astrophysical Journal, 904, 144

——. 2023, CEERS: Diversity of Lyman-Alpha Emitters during the Epoch of Reionization

——. 2022, New \z \textgreater 7\ Lyman-alpha Emitters in EGS: Evidence of an Extended Ionized Structure at \z \textbackslashsim 7.7\

Juodžbalis, I. et al. 2023, Monthly Notices of the Royal Astronomical Society, 525, 1353, arXiv:2307.07535 [astro-ph]

Kannan, R., Garaldi, E., Smith, A., Pakmor, R., Springel, V., Vogelsberger, M., & Hernquist, L. 2021, arXiv:2110.00584 [astro-ph]

Kashikawa, N. et al. 2006, The Astrophysical Journal, 648, 7

——. 2011, The Astrophysical Journal, 734, 119

Kimble, R. A., J. MacKenty, O'Connell, R. W., & Townsend, J. A. 2008, Proc. SPIE, 7010

Kistler, M. D., Yüksel, H., Beacom, J. F., Hopkins, A. M., & Wyithe, J. S. B. 2009, ApJ, 705, L104

Konno, A. et al. 2014, ApJ, 797, 16

Kornei, K. A., Shapley, A. E., Erb, D. K., Steidel, C. C., Reddy, N. A., Pettini, M., & Bogosavljević, M. 2010, ApJ, 711, 693

Kriek, M. et al. 2015, ApJS, 218, 15

Kroupa, P., & Boily, C. M. 2002, Monthly Notices of the Royal Astronomical Society, 336, 1188

Kulkarni, G., Worseck, G., & Hennawi, J. F. 2019, Monthly Notices of the Royal Astronomical Society, 488, 1035

Kusakabe, H. et al. 2020, A&A, 638, A12

Larson, R. L. et al. 2022, ApJ, 930, 104

——. 2023, ApJL, 953, L29

Laursen, P., Sommer-Larsen, J., Milvang-Jensen, B., Fynbo, J. P. U., & Razoumov, A. O. 2019, A&A, 627, A84

Le Fèvre, O. et al. 2015, A&A, 576, A79

Lemaux, B. C. et al. 2022, A&A, 662, A33

——. 2021, Monthly Notices of the Royal Astronomical Society, 504, 3662

——. 2009, The Astrophysical Journal, 700, 20

Lin, Y.-H. et al. 2023, An Empirical reionization history model inferred from star-forming galaxies at \z\textgreater8\

Livermore, R. C., Finkelstein, S. L., & Lotz, J. M. 2017, The Astrophysical Journal, 835, 113

Llerena, M. et al. 2022, A&A, 659, A16

Lotz, J. M. et al. 2017, The Astrophysical Journal, 837, 97

Marchi, F. et al. 2018, Astronomy & Astrophysics, 614, A11

——. 2019, A&A, 631, A19

Martin, J. 2018, The Theory of Inflation, arXiv:1807.11075 [astro-ph, physics:gr-qc, physics:hep-th]

Mascia, S. et al. 2023a, New insight on the nature of cosmic reionizers from the CEERS survey

——. 2023b, A&A, 672, A155

Maseda, M. V. et al. 2023, JWST/NIRSpec Measurements of Extremely Low Metallicities in High Equivalent Width Lyman-{\textbackslashalpha\ Emitters

Mason, C. A. et al. 2019a, Monthly Notices of the Royal Astronomical Society, 485, 3947

Mason, C. A., Naidu, R. P., Tacchella, S., & Leja, J. 2019b, Monthly Notices of the Royal Astronomical Society, 489, 2669

Mason, C. A., Trenti, M., & Treu, T. 2015, The Astrophysical Journal, 813, 21

Mason, C. A., Treu, T., Dijkstra, M., Mesinger, A., Trenti, M., Pentericci, L., De Barros, S., & Vanzella, E. 2018, ApJ, 856, 2

Matthee, J., Sobral, D., Darvish, B., Santos, S., Mobasher, B., Paulino-Afonso, A., Röttgering, H., & Alegre, L. 2017, Monthly Notices of the Royal Astronomical Society, 472, 772

McCarron, A. P. et al. 2022, ApJ, 936, 131

McGreer, I. D., Mesinger, A., & D'Odorico, V. 2015, Monthly Notices of the Royal Astronomical Society, 447, 499

McLean, I. S. et al. 2010, San Diego, California, USA, 77351E

McQuinn, M. 2016, Annu. Rev. Astron. Astrophys., 54, 313

McQuinn, M., Hernquist, L., Zaldarriaga, M., & Dutta, S. 2007, Monthly Notices of the Royal Astronomical Society, 381, 75

Merlin, E. et al. 2015, Astronomy & Astrophysics, 582, A15

Mesinger, A., Aykutalp, A., Vanzella, E., Pentericci, L., Ferrara, A., & Dijkstra, M. 2015, Monthly Notices of the Royal Astronomical Society, 446, 566

Mesinger, A., Furlanetto, S., & Cen, R. 2011, Monthly Notices of the Royal Astronomical Society, 411, 955

Mesinger, A., Greig, B., & Sobacchi, E. 2016, Monthly Notices of the Royal Astronomical Society, 459, 2342

Miralda-Escude, J. 1998, The Astrophysical Journal, 501, 15

Mo, H., van den Bosch, F., & White, S. 2010, Galaxy Formation and Evolution (Cambridge University Pressa)

Morales, A., Mason, C., Bruton, S., Gronke, M., Haardt, F., & Scarlata, C. 2021, arXiv:2101.01205 [astro-ph]

Morishita, T. et al. 2023, ApJL, 947, L24

Naidu, R. P., Forrest, B., Oesch, P. A., Tran, K.-V. H., & Holden, B. P. 2018, Monthly Notices of the Royal Astronomical Society, 478, 791

Naidu, R. P. et al. 2022, Monthly Notices of the Royal Astronomical Society, 510, 4582

Naidu, R. P., Tacchella, S., Mason, C. A., Bose, S., Oesch, P. A., & Conroy, C. 2020, The Astrophysical Journal, 892, 109

Nakajima, K., Fletcher, T., Ellis, R. S., Robertson, B. E., & Iwata, I. 2018a, Monthly Notices of the Royal Astronomical Society, 477, 2098

Nakajima, K., Ouchi, M., Isobe, Y., Harikane, Y., Zhang, Y., Ono, Y., Umeda, H., & Oguri, M. 2023, ApJS, 269, 33

Nakajima, K. et al. 2018b, A&A, 612, A94

Napolitano, L. et al. 2023, Identifying Ly{\textbackslashalpha} emitter candidates with Random Forest: learning from galaxies in CANDELS survey

Nilsson, K. K., Orsi, A., Lacey, C. G., Baugh, C. M., & Thommes, E. 2007, A&A, 474, 385

Nilsson, K. K., Östlin, G., Møller, P., Möller-Nilsson, O., Tapken, C., Freudling, W., & Fynbo, J. P. U. 2011, A&A, 529, A9

Oke, J. B., & Gunn, J. E. 1983, ApJ, 266, 713

Ono, Y. et al. 2012, The Astrophysical Journal, 744, 83

Orsi, A., Fanidakis, N., Lacey, C. G., & Baugh, C. M. 2016, Mon. Not. R. Astron. Soc., 456, 3827

Ortiz, O. A. C. et al. 2023, Introducing the Texas Euclid Survey for Lyman Alpha (TESLA) Survey: Initial Study Correlating Galaxy Properties to Lyman-Alpha Emission

Ouchi, M. et al. 2005, ApJ, 635, L117

——. 2018, Publications of the Astronomical Society of Japan, 70

——. 2010, The Astrophysical Journal, 723, 869

Oyarzún, G. A., Blanc, G. A., González, V., Mateo, M., & Bailey, J. I. 2017, The Astrophysical Journal, 843, 133

Oyarzún, G. A. et al. 2016, The Astrophysical Journal, 821, L14

Pahl, A. J., Shapley, A., Steidel, C. C., Chen, Y., & Reddy, N. A. 2021, Monthly Notices of the Royal Astronomical Society, 505, 2447

Pedregosa, F. et al. 2018, arXiv:1201.0490 [cs]

Peebles, P. J. E. 1968, ApJ. . ., 153

Pelliccia, D. et al. 2021, The Astrophysical Journal Letters, 908, L30

Pentericci, L. et al. 2011, The Astrophysical Journal, 743, 132

Pentericci, L., Grazian, A., Fontana, A., Castellano, M., Giallongo, E., Salimbeni, S., & Santini, P. 2009, A&A, 494, 553

Pentericci, L., Grazian, A., Fontana, A., Salimbeni, S., Santini, P., De Santis, C., Gallozzi, S., & Giallongo, E. 2007, A&A, 471, 433

Pentericci, L. et al. 2018, A&A, 619, A147

——. 2014, The Astrophysical Journal, 793, 113

Perez, F., & Granger, B. E. 2007, Computing in Science Engineering, 9, 21

Planck Collaboration et al. 2016, Astronomy & Astrophysics, 594, A28

——. 2020, A&A, 641, A6

Postman, M. et al. 2012, The Astrophysical Journal Supplement Series, 199, 25

Prieto-Lyon, G. et al. 2022, The production of ionizing photons in UV-faint z\textasciitilde3-7 galaxies

Pucha, R., Reddy, N. A., Dey, A., Juneau, S., Lee, K.-S., Prescott, M. K. M., Shivaei, I., & Hong, S. 2022, AJ, 164, 159

Qin, Y., Wyithe, J. S. B., Oesch, P. A., Illingworth, G. D., Leonova, E., Mutch, S. J., & Naidu, R. P. 2022, Monthly Notices of the Royal Astronomical Society, 510, 3858, arXiv:2108.03675 [astro-ph]

Reddy, N. A. et al. 2018, The Astrophysical Journal, 853, 56

——. 2022, ApJ, 926, 31

Robertson, B. E. 2021, arXiv:2110.13160 [astro-ph]

Robertson, B. E., Ellis, R. S., Furlanetto, S. R., & Dunlop, J. S. 2015, The Astrophysical Journal, 802, L19

Robertson, B. E. et al. 2023, Nat Astron, 7, 611

Rosdahl, J. et al. 2022, Monthly Notices of the Royal Astronomical Society, 515, 2386

Rossi, A. et al. 2022, A&A, 665, A125

Saldana-Lopez, A. et al. 2023, Monthly Notices of the Royal Astronomical Society, 522, 6295

Salim, S., Boquien, M., & Lee, J. C. 2018, ApJ, 859, 11

Sanders, R. L., Shapley, A. E., Topping, M. W., Reddy, N. A., & Brammer, G. B. 2023, ApJ, 955, 54

Santos, S. et al. 2020, arXiv:1910.02959 [astro-ph], arXiv: 1910.02959

Saxena, A. et al. 2023a, JADES: The production and escape of ionizing photons from faint Lyman-alpha emitters in the epoch of reionization

——. 2023b, JADES: Discovery of extremely high equivalent width Lyman-alpha emission from a faint galaxy within an ionized bubble at z=7.3

Schenker, M. A., Ellis, R. S., Konidaris, N. P., & Stark, D. P. 2014, The Astrophysical Journal, 795, 20

Schenker, M. A., Stark, D. P., Ellis, R. S., Robertson, B. E., Dunlop, J. S., McLure, R. J., Kneib, J.-P., & Richard, J. 2012, The Astrophysical Journal, 744, 179

Scholtz, J. et al. 2023, GN-z11: The environment of an AGN at \z=\10.603

Schroeder, J., Mesinger, A., & Haiman, Z. 2013, Monthly Notices of the Royal Astronomical Society, 428, 3058

Seeyave, L. T. C. et al. 2023, Monthly Notices of the Royal Astronomical Society, 525, 2422

Shapley, A. E., Reddy, N. A., Sanders, R. L., Topping, M. W., & Brammer, G. B. 2023, ApJL, 950, L1

Sharma, M., Theuns, T., Frenk, C., Bower, R., Crain, R., Schaller, M., & Schaye, J. 2016, Mon. Not. R. Astron. Soc: Lett., 458, L94

Shipley, H. V. 2018, The Astrophysical Journal Supplement Series

Silva, L., Granato, G. L., Bressan, A., & Danese, L. 1998, ApJ, 509, 103

Simmonds, C. et al. 2023, Low-mass bursty galaxies in JADES efficiently produce ionising photons and could represent the main drivers of reionisation, arXiv:2310.01112 [astro-ph]

Sirianni, M. et al. 2005, PUBL ASTRON SOC PAC, 117, 1049

Smith, A., Kannan, R., Garaldi, E., Vogelsberger, M., Pakmor, R., Springel, V., & Hernquist, L. 2021, arXiv:2110.02966 [astro-ph]

Sobacchi, E., & Mesinger, A. 2014, Monthly Notices of the Royal Astronomical Society, 440, 1662

——. 2015, Monthly Notices of the Royal Astronomical Society, 453, 1843

Sobral, D., Matthee, J., Darvish, B., Schaerer, D., Mobasher, B., Röttgering, H. J. A., Santos, S., & Hemmati, S. 2015, ApJ, 808, 139

Sobral, D. et al. 2018, Monthly Notices of the Royal Astronomical Society, 477, 2817

Stark, D. P., Ellis, R. S., Chiu, K., Ouchi, M., & Bunker, A. 2010, Monthly Notices of the Royal Astronomical Society, 408, 1628

Stark, D. P. et al. 2015, Monthly Notices of the Royal Astronomical Society, 450, 1846

——. 2014, Monthly Notices of the Royal Astronomical Society, 445, 3200

Steidel, C., Giavalisco, M., Pettini, M., Dickinson, M., & Adelberger, K. 1996, ApJ, 462, L17, arXiv:astro-ph/9602024

Steidel, C. C., Bogosavljević, M., Shapley, A. E., Reddy, N. A., Rudie, G. C., Pettini, M., Trainor, R. F., & Strom, A. L. 2018, The Astrophysical Journal, 869, 123

Steidel, C. C., Strom, A. L., Pettini, M., Rudie, G. C., Reddy, N. A., & Trainor, R. F. 2016, ApJ, 826, 159

Strait, V. et al. 2020, The Astrophysical Journal, 888, 124

——. 2018, ApJ, 868, 129

Tacchella, S. et al. 2023, Monthly Notices of the Royal Astronomical Society, 522, 6236

Tang, M. et al. 2023, JWST/NIRSpec Spectroscopy of \z=7-9\ Star Forming Galaxies with CEERS: New Insight into Bright Ly{\textbackslashalpha\ Emitters in Ionized Bubbles

Tang, M., Stark, D. P., Chevallard, J., & Charlot, S. 2019, Monthly Notices of the Royal Astronomical Society, 489, 2572

Tang, M., Stark, D. P., Chevallard, J., Charlot, S., Endsley, R., & Congiu, E. 2021, Monthly Notices of the Royal Astronomical Society, 501, 3238

Tasca, L. A. M. et al. 2017, A&A, 600, A110

Tee, W. L., Fan, X., Wang, F., Yang, J., Malhotra, S., & Rhoads, J. E. 2023, Predicting the Yields of z > 6.5 Quasar Surveys in the Era of Roman and Rubin, arXiv:2308.12278 [astro-ph]

The Astropy Collaboration et al. 2018, AJ, 156, 123

Tilvi, V. et al. 2014, The Astrophysical Journal, 794, 5

Topping, M. W., Shapley, A. E., Stark, D. P., Endsley, R., Robertson, B., Greene, J. E., Furlanetto, S. R., & Tang, M. 2021, ApJL, 917, L36

Totani, T., Kawai, N., Kosugi, G., Aoki, K., Yamada, T., Iye, M., Ohta, K., & Hattori, T. 2006, Publ Astron Soc Jpn, 58, 485

Trac, H., Cen, R., & Loeb, A. 2008, The Astrophysical Journal, 689, L81

Trainor, R. F., Strom, A. L., Steidel, C. C., Rudie, G. C., Chen, Y., & Theios, R. L. 2019, ApJ, 887, 85

Trancho, G. 2022

Treu, T. et al. 2022, ApJ, 935, 110

Treu, T., Schmidt, K. B., Trenti, M., Bradley, L. D., & Stiavelli, M. 2013, ApJ, 775, L29

Treu, T., Trenti, M., Stiavelli, M., Auger, M. W., & Bradley, L. D. 2012, ApJ, 747, 27

Trinca, A., Schneider, R., Valiante, R., Graziani, L., Ferrotti, A., Omukai, K., & Chon, S. 2023, Exploring the nature of UV-bright $z \gtrsim 10$ galaxies detected by JWST: star formation, black hole accretion, or a non universal IMF?, arXiv:2305.04944 [astro-ph]

Trump, J. R. et al. 2023, ApJ, 945, 35

Trussler, J. A. A. et al. 2023, Monthly Notices of the Royal Astronomical Society, 523, 3423

Tsujikawa, S. 2003, Introductory review of cosmic inflation, arXiv:hep-ph/0304257

van der Walt, S., Colbert, S. C., & Varoquaux, G. 2011, Computing in Science Engineering, 13, 22

Vanzella, E. et al. 2016, ApJ, 825, 41

——. 2011, ApJ, 730, L35

Verhamme, A., Schaerer, D., Atek, H., & Tapken, C. 2008, A&A, 491, 89

Wang, F. et al. 2020, The Astrophysical Journal, 896, 23

Whitler, L. R., Mason, C. A., Ren, K., Dijkstra, M., Mesinger, A., Pentericci, L., Trenti, M., & Treu, T. 2020, Monthly Notices of the Royal Astronomical Society, 495, 3602

Willott, C. J. et al. 2022, PASP, 134, 025002

Witstok, J. et al. 2023, Inside the bubble: exploring the environments of reionisation-era Lyman-{\textbackslashalpha} emitting galaxies with JADES and FRESCO

Wold, I. G. B. et al. 2022, arXiv:2105.12191 [astro-ph], arXiv: 2105.12191

Wong, T. 2009, The Astrophysical Journal, 705, 650

Wong, W. Y. 2008, Cosmological Recombination, arXiv:0811.2826 [astro-ph]

Yamanaka, S., & Yamada, T. 2019, Publications of the Astronomical Society of Japan, 71, 51

Yan, H. 2004, 600, 5

Yang, H. et al. 2017, ApJ, 844, 171

Yeh, J. Y.-C. et al. 2023, Monthly Notices of the Royal Astronomical Society, 520, 2757

Zhu, Y. et al. 2021, The Astrophysical Journal, 923, 223

——. 2022, Long Dark Gaps in the Lyβ Forest at $z<6$: Evidence of Ultra Late Reionization from XQR-30 Spectra, Tech. Rep. arXiv:2205.04569, arXiv, arXiv:2205.04569 [astro-ph] type: article

Zwicky, F. 1937, Physical Review journals, 51, 290